浙江大学聚变理论与模拟中心
Institute for Fusion Theory and Simulation, Zhejiang University

A simple model for internal transport barrier induced by fishbone in tokamak plasmas

Guoyong Fu, Zhaoyang Liu*, Peiyou Jiang, Shiyang Liu, Jian Bao**

Institute for Fusion Theory and Simulation (IFTS),
School of Physics, Zhejiang University, Hangzhou, China
*Zhejiang Laboratory, Hangzhou, China
**Institute of Physics, CAS, Beijing, China

PPPL seminar, Oct 18, 2024

Zhejiang University is located in Hangzhou, the capital of Zhejiang province

Zhejiang University is a top university in China and beyond

Introduction to Institute for Fusion Theory and Simulation

We carry out frontier research in magnetic confinement fusion and high energy density physics mainly using theory and simulation. We have 8 faculty members and more than 30 graduate students.

Magnetic Confinement Fusion

Prof. Liu Chen

Prof. Guoyong Fu

Prof. Zhiwei Ma

Prof. Yong Xiao

Dr. Wei Zhang

High Energy Density Physics

Prof. Zhengmao Sheng

Prof. Hui-Chun Wu

Dr. Xinglong Zhu

Introduction to Institute for Fusion Theory and Simulation

Key Research Areas

- **Magnetic Confinement Fusion**

  Energetic Particle Physics: **Energetic particle-driven instabilities and transport, interaction with thermal plasmas**

  MHD instabilities: tokamak sawteeth, tearing modes, density limit

  Micro-turbulence and transport: burning plasma transport, gyrokinetic simulation, AI fusion

  Stellarator: stellarator design and optimization

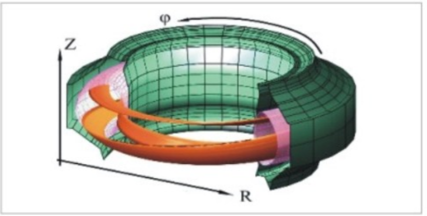

托卡马克中磁流体不稳定性引起的磁面变化

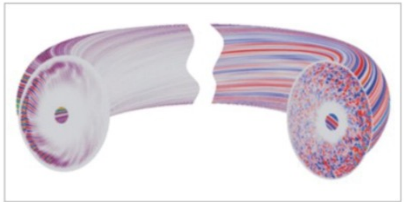

托卡马克中的微观湍流的线性(左)和非线性(右)

- **High Energy Density Physics**

  The physics of warm dense matter: Inertial Confinement Fusion (ICF), Ion beam targeting fusion, laser plasma interaction and particle acceleration

  The physics of strong fields: Relativistic discharges, Relativistic electromagnetic waves, Strong-field QED effects, Novel radiation sources

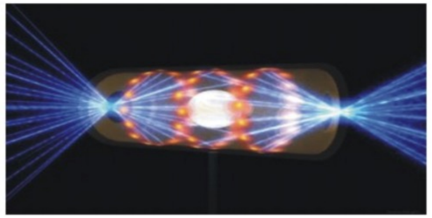

间接驱动惯性约束聚变示意图

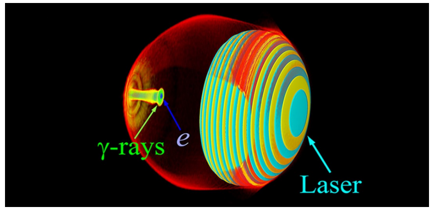

Laser acceleration and radiation

Outline

- Background
- A simple model for fishbone-induced ITB
- Numerical results
- Summary and conclusions
- Update on hybrid code GMEC

Background

- Fishbone [1]

[1] K. McGuire et al., PRL 1983; L. Chen et al., PRL 1984;

B. Coppi et al., PRL 1986

- Internal transport barrier（ITB）[2]

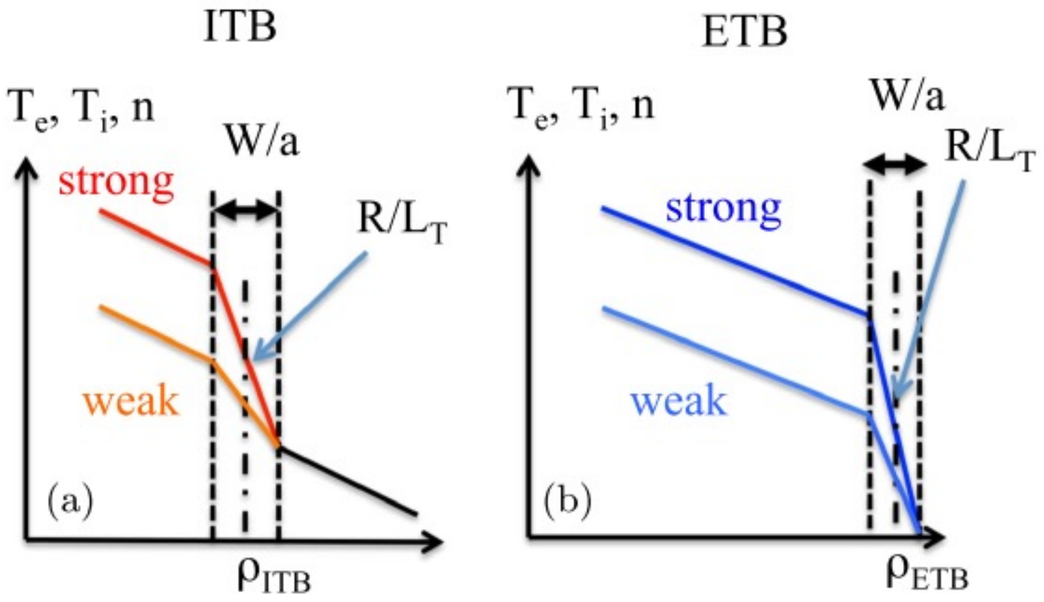

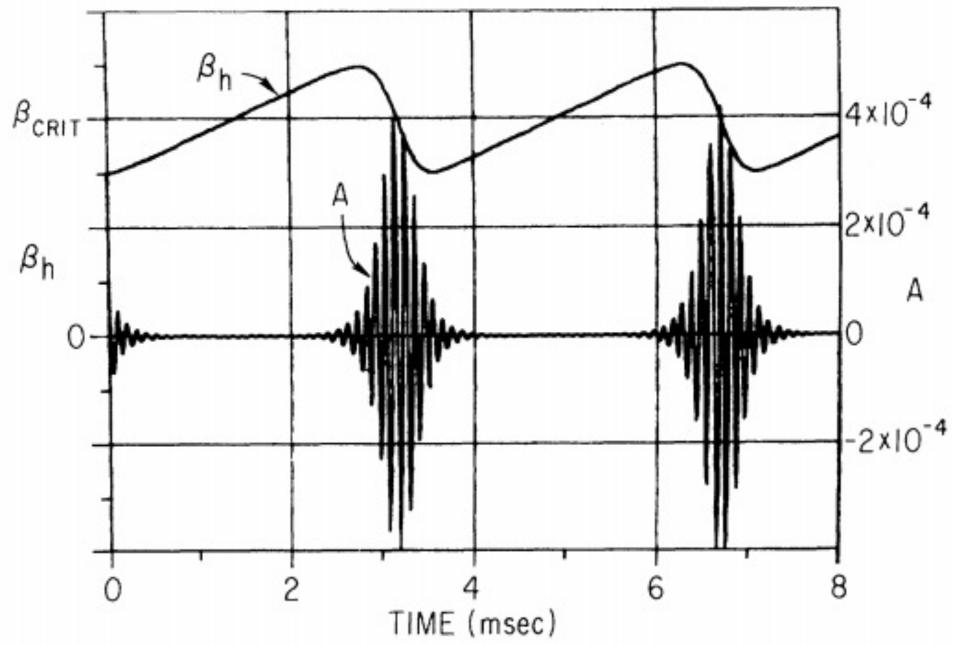

FIG. 1. The kink-mode amplitude, $A(t)\cos(\bar{\omega}_{dh}t)$, and the beam-particle beta, $\beta_h(t)$, vs time as obtained from Eqs. (13) and (14), for PDX parameters.

[2] K. Ida and T. Fujita, Internal transport barrier in tokamak and helical plasmas, Plasma Phys. Control. Fusion 60, 033001 (2018)

Physics of fishbone-induced ITB

Fishbone → EP radial current → plasma return current

→ plasma rotation → suppression of turbulence → ITB formation

Background: ASDEX-U experiments

✓ Fishbone is favorable for stationary discharge [1]

[1] R. C. Wolf, O. Gruber, M. Maraschek, et. al.,, "Stationary advanced scenarios with internal transport barrier on ASDEX Upgrade", Plasma Phys. Control. Fusion 41, B93 (1999)

✓ Responsible for clamping q to the vicinity of unity and avoiding sawteeth [2]

[2] O. Gruber, R. Wolf, H.-S. Bosch, et. al., "Steady state H mode and Te≈Ti operation with internal transport barriers in ASDEX Upgrade", Nucl. Fusion 40, 1145 (2000)

✓ Redistribution of the resonant EPs resulting in a sheared plasma rotation [3]

[3] S. Gunter, A. Gude, J. Hobirk, et. al., "MHD phenomena in advanced scenarios on ASDEX Upgrade and the influence of localized electron heating and current drive", Nucl. Fusion 41, 1283 (2001)

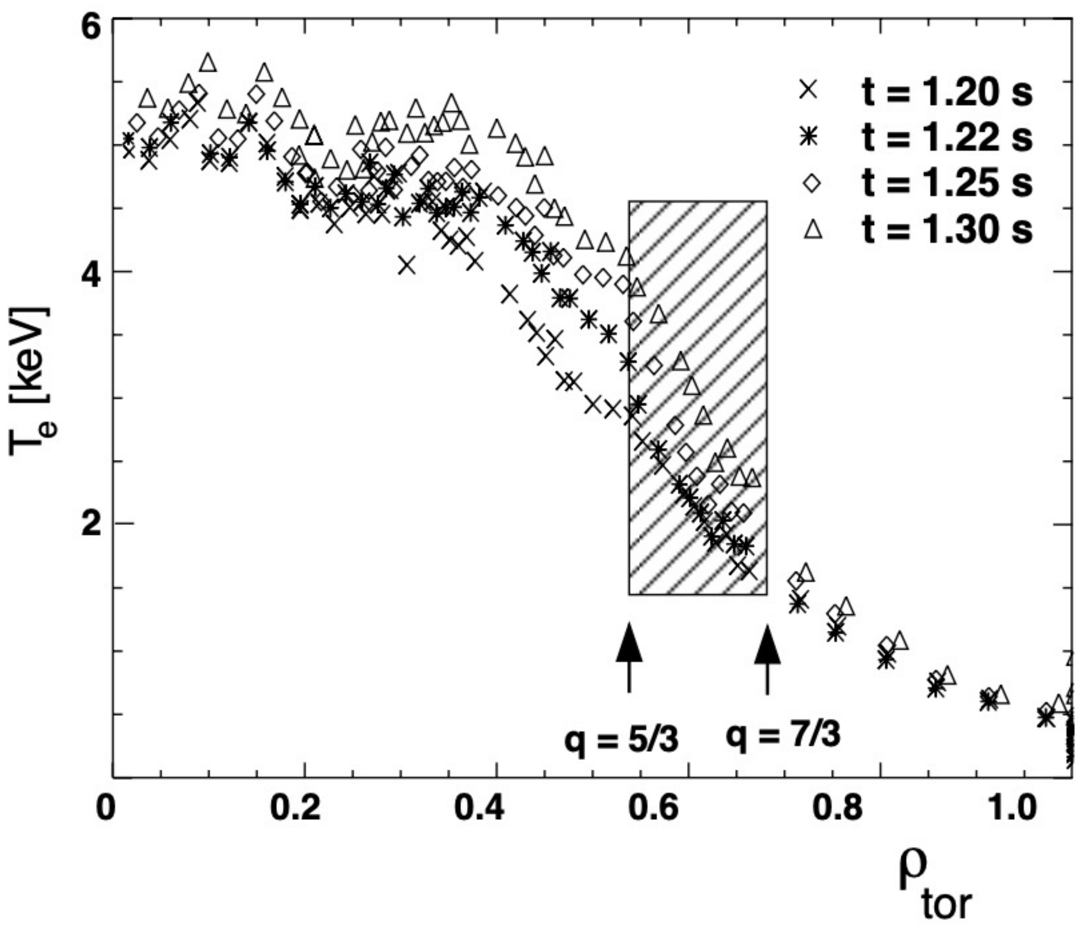

Background: EAST experiments

✓ ITB formation is stepwise and always appears after the fishbone instability [1]

[1] Y. Yang, X. Gao, H. Q. Liu, et. al., "Observation of internal transport barrier in ELMy H-mode plasmas on the EAST tokamak", Plasma Phys. Control. Fusion 59, 085003 (2017)

✓ Large E×B zonal flow can be induced in the nonlinear fishbone stage [2]

[2] Z. X. Liu, W. L. Ge, F. Wang, et. al., "Experimental observation and simulation analysis of the relationship between the fishbone and ITB formation on EAST tokamak", Nucl. Fusion 60, 122001 (2020)

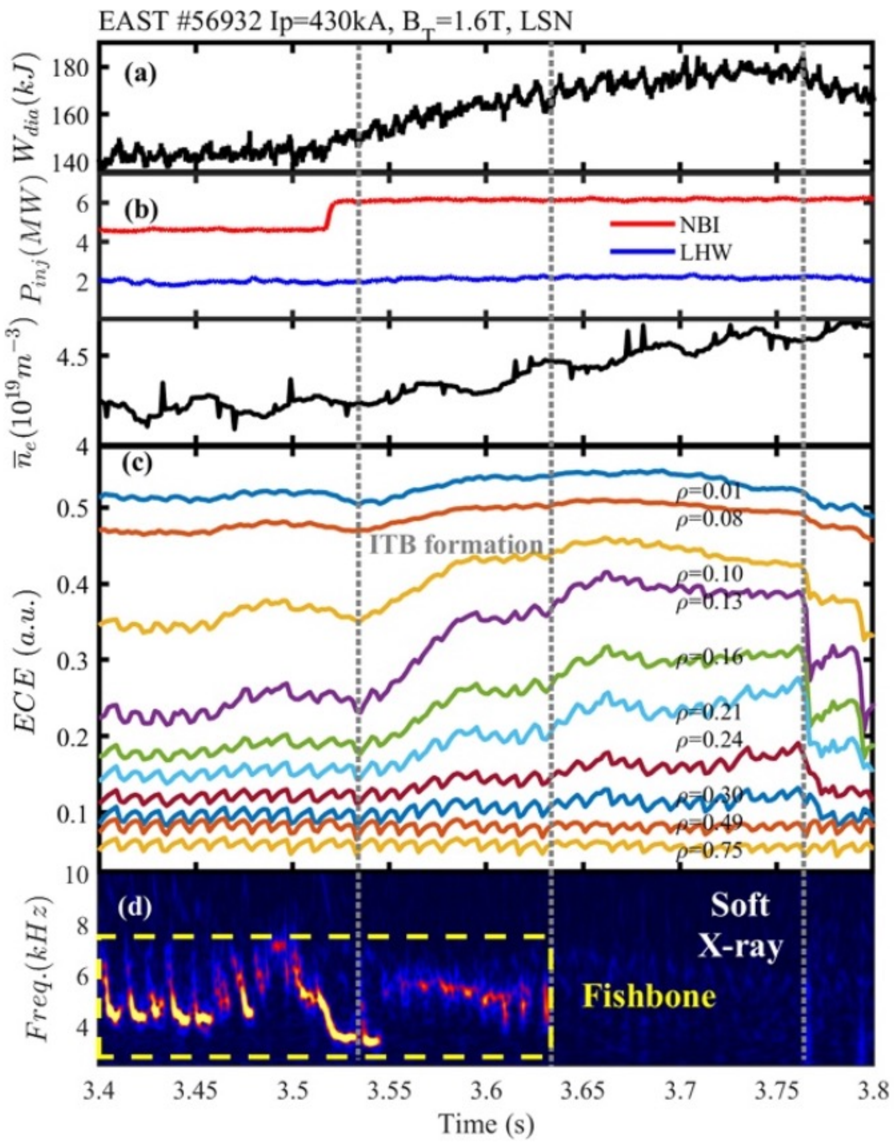

Background: EAST experiments

✓ ITB formation in the ion thermal channel strongly correlates to the excitation of the fishbone [3]

[3] B. Zhang , X. Gong, J. Qian, et. al., "Progress on physics understanding of improved confinement with fishbone instability at low q95 < 3.5 operation regime in EAST", Nucl. Fusion 62, 126064 (2022)

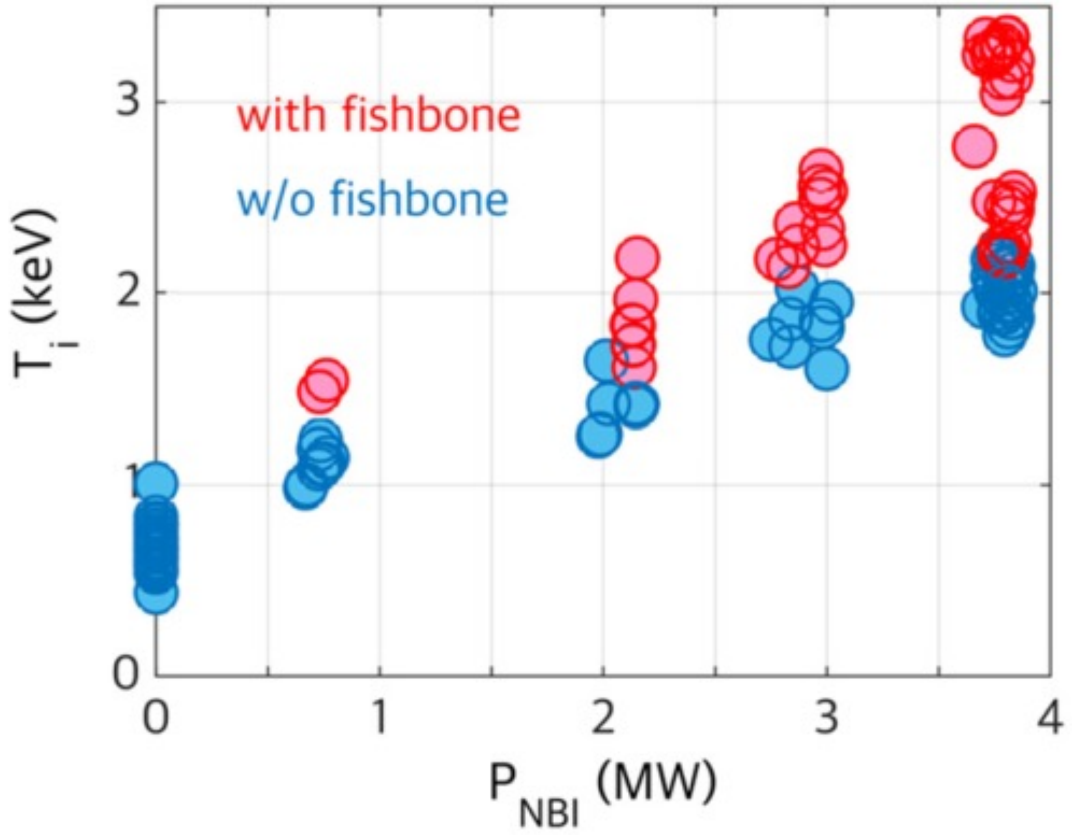

Background: theory and simulation

- Quasi-linear theory [1]

[1] V. V. Lutsenko and V. S. Marchenko, “Self-consistent model for the radial current generation during fishbone activity”, Phys. Plasmas 9, 4819 (2002)

ASDEX-Upgrade: HAGIS [2]

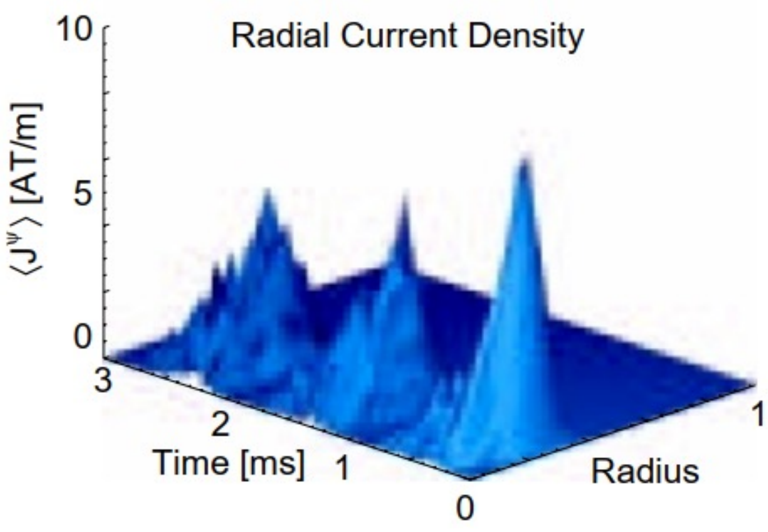

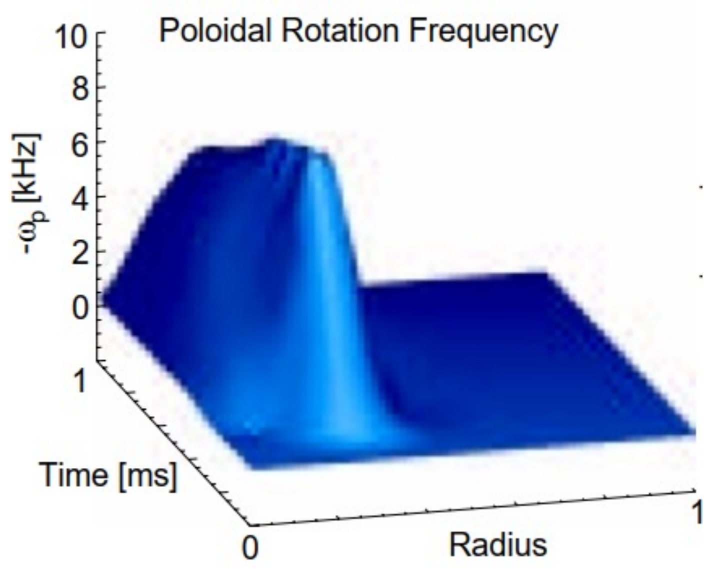

[2] S. D. Pinches, S. Gunter, A. G. Peeters and the ASDEX Upgrade Team, “Fishbone Generation of Sheared Flows and the Creation of Transport Barriers”, ECA Vol. 25A, 57–60 (2001)

Background: GTC simulation of fishbone

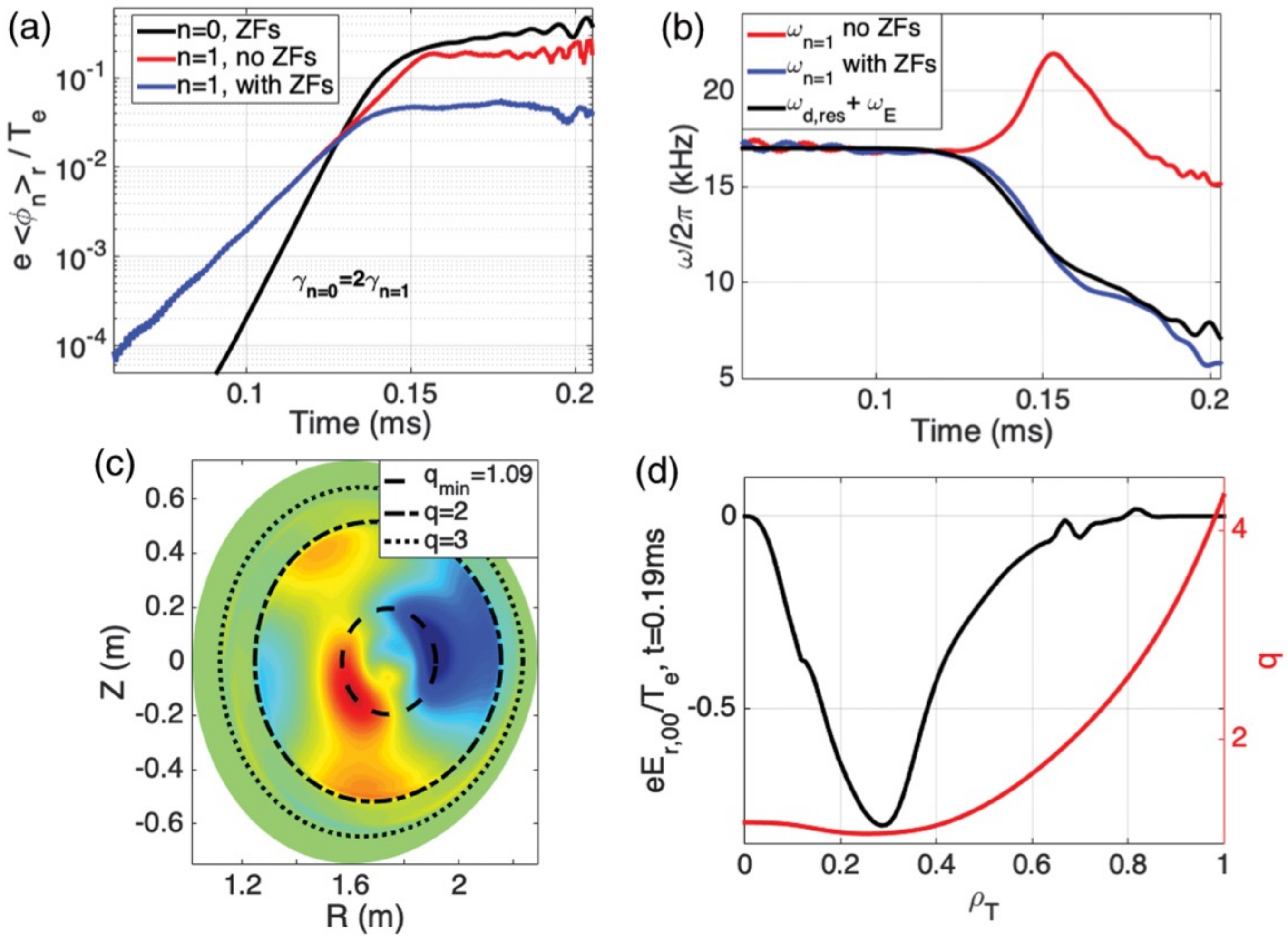

[1] G. Brochard, C. Liu, X. Wei, et. al., “Saturation of fishbone modes by self-generated zonal flows in tokamak plasmas”, PHYSICAL REVIEW LETTERS 132, 075101 (2024)

Theoretical model: Fishbone amplitude evolution equation

- Predator-prey model [1]

$$\frac{d\beta_{ep}}{dt} = D - AZ\beta_{max}H\left(\beta_{ep} - \beta_{min}\right),$$

$$\frac{dA}{dt} = A\Gamma\left(\beta_{ep} - \beta_{crit}\right),$$

[1] R. B. White et al, Phys. Fluids 26, 2958 (1983)

$$\beta_{max} = \beta_{crit} / \left(1 - f_t / 2\right),\ \beta_{min} = \left(1 - f_t\right)\beta_{max}$$

- Five free parameters $D, Z, \beta_{crit}, \beta_{max}, \Gamma$

Theoretical model: Fishbone amplitude evolution equation

- Predator-prey model [1]

$$\frac{d\beta_{ep}}{dt} = D - AZ\beta_{max}H\left(\beta_{ep} - \beta_{min}\right),$$

$$\frac{dA}{dt} = A\Gamma\left(\beta_{ep} - \beta_{crit}\right),$$

[1] R. B. White et al, Phys. Fluids 26, 2958 (1983)

$$\beta_{max} = \beta_{crit} / \left(1 - f_t / 2\right),\ \beta_{min} = \left(1 - f_t\right)\beta_{max}$$

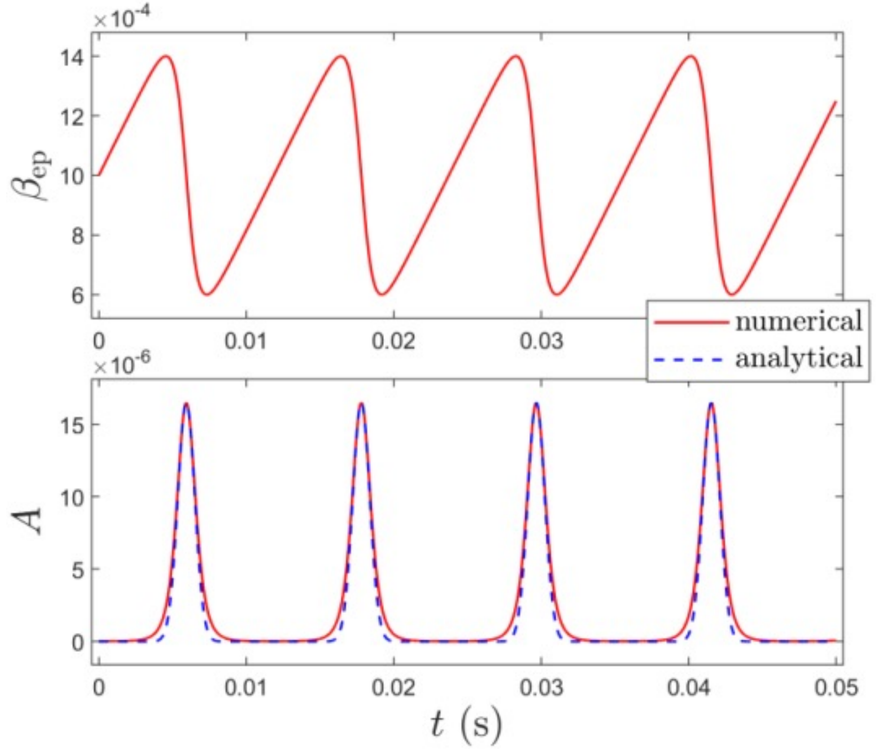

Theoretical model: Fishbone amplitude evolution equation

- Predator-prey model [1]

$$\frac{d\beta_{ep}}{dt} = D - AZ\beta_{max}H\left(\beta_{ep} - \beta_{min}\right),$$

$$\frac{dA}{dt} = A\Gamma\left(\beta_{ep} - \beta_{crit}\right),$$

[1] R. B. White et al, Phys. Fluids 26, 2958 (1983)

- Steady solution

$$\mathcal{H}\left(x, p_x\right) \equiv \frac{1}{2}\Gamma p_x^2 - Dx + e^x Z\beta_{max} = C, \quad J = \oint p_x dx$$

$$x \equiv \ln A$$

$$p_x \equiv \beta_{ep} - \beta_{crit}$$

- Five free parameters

$$D, Z, \beta_{crit}, \beta_{max}, \Gamma$$

Theoretical model: Fishbone amplitude evolution equation

- Predator-prey model

- Burst period

$$t_p = \frac{dJ}{dC} = \sqrt{\frac{2}{\Gamma}} \int_{A_{\min}}^{A_{\max}} dA \frac{1}{A\sqrt{\left(A_{\max} - A\right) Z\beta_{\max} - D\ln\left(A_{\max} / A\right)}} 。$$

- Burst width

$$A_s(t) \approx A_{\max} \exp\left[-\left(\frac{t-t_0}{\Delta t}\right)^2\right], \quad \Delta t = \sqrt{\frac{2}{\Gamma\left(A_{\max} Z\beta_{\max} - D\right)}},$$

- Approximate solution

$$A(t) = \sum_{p=0,1,2,\ldots} A_s\left(t - pt_p\right) H\left(t - pt_p\right) H\left(\left(p+1\right)t_p - t\right) 。$$

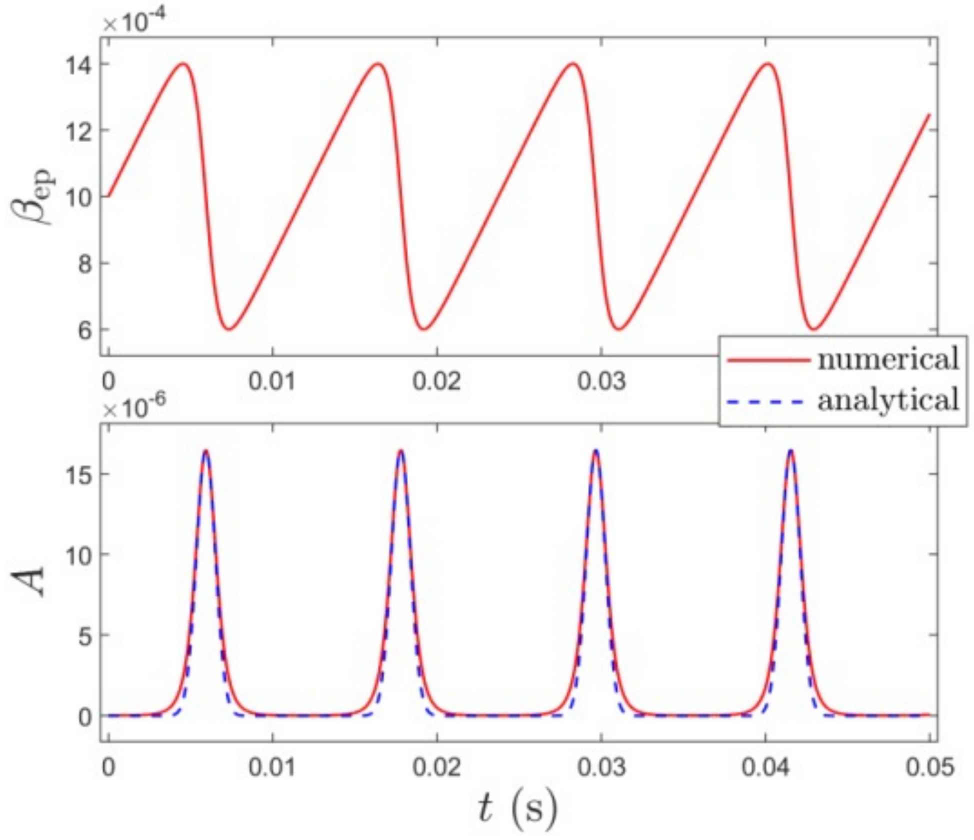

Theoretical model: Fishbone amplitude evolution equation

- Numerical solution, initial condition $\beta_{ep} = \beta_{crit}$, $A = A_{min}$ 。

- Parameters [1] $\beta_{crit} = 0.001$, $\beta_{max} = 0.0014$, $\Gamma = 5.0\times10^6/s$, $D = 0.1/s$, $Z = 3.0\times10^7/s$ 。

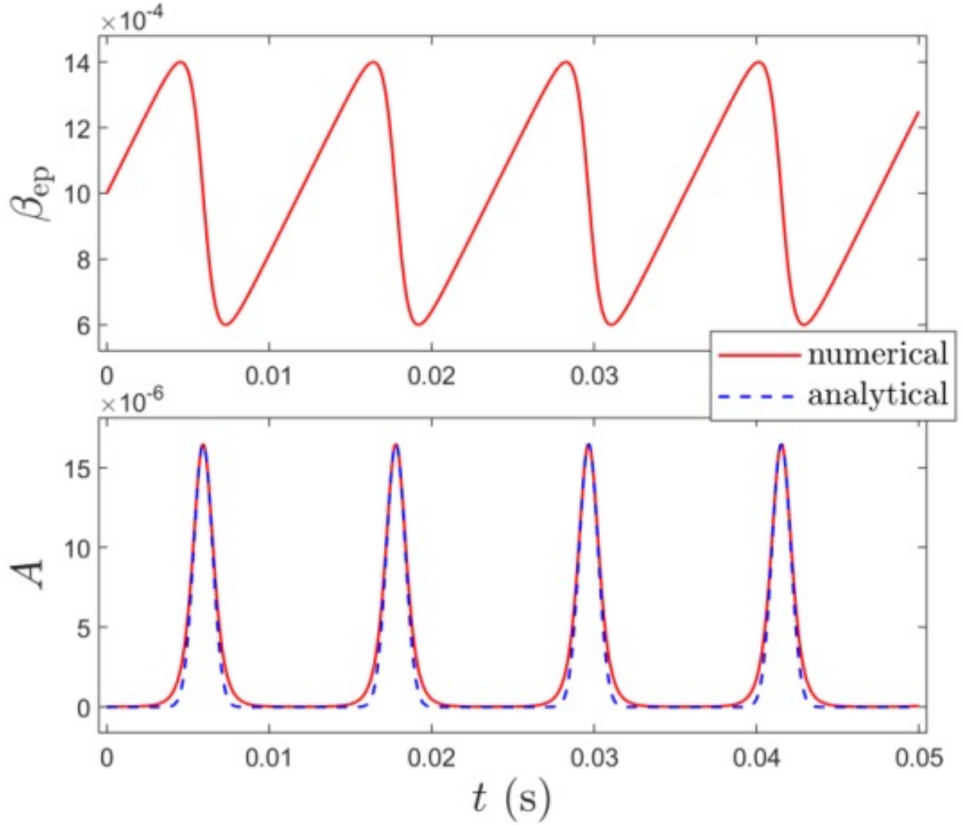

[1] X. Zhu, L. Zeng, Z. Y. Qiu, et. al., Dependence of fishbone cycle on energetic particle intensity in EAST low-magnetic-shear plasmas. J. Plasma Phys. vol. 86, 905860610 (2020)

Theoretical model: EP radial current

- The flux surface averaged EP charge conservation law

$$\frac{d\rho_{\mathrm{ep}}}{dt}+\frac{1}{r}\frac{\partial}{\partial r}(rJ_r)=S_{\mathrm{ep}},$$

- Radial structure represented by a Gaussian shape

$$J_r(r,t)\approx J(t)\frac{r}{r_s}\exp\left[-\left(\frac{r-r_s}{\Delta r}\right)^2\right],$$

- Integrating from 0 to r_s

$$\frac{d\beta_{\mathrm{ep}}}{dt}=D-\frac{2\mu_0 T_{\mathrm{ep}}}{B_0^2 q_{\mathrm{ep}} r_s}J(t),$$

- Radial current is proportional to the fishbone amplitude

$$J(t)=J_f A(t),\quad J_f\equiv\frac{B_0^2 q_{\mathrm{ep}} r_s}{2\mu_0 T_{\mathrm{ep}}}Z\beta_{\max}\circ$$

Theoretical model: Poloidal rotation driven by EP radial current

- Radial current is proportional to the fishbone amplitude

$$J(t) = J_f A(t), \quad J_f \equiv \frac{B_0^2 q_{\mathrm{ep}} r_s}{2\mu_0 T_{\mathrm{ep}}} Z \beta_{\max} 。$$

$$J_r(r,t) \approx J(t) \frac{r}{r_s} \exp\left[-\left(\frac{r - r_s}{\Delta r} \right)^2 \right],$$

\

- Poloidal rotation driven by radial current [1]

$$a \frac{\partial V_\theta}{\partial t} = -\nu V_\theta - f J_r \ ,$$

[1] A. G. Peeters, Phys Plasmas 5, 763 (1998)

$$a = \left(\varepsilon^2 / q^2\right)\left(1 + 2q^2 + 1.63 q^2 / \sqrt{\varepsilon}\right),$$

$$\nu = 1.1 \nu_{ii} \sqrt{\varepsilon} \, , \ f = \left(\varepsilon^2 / q^2\right)\left(B_0 / n_i m_i\right)$$

Theoretical model: Poloidal rotation driven by EP radial current

- Steady solution for poloidal flow and its radial shear

$$\frac{\partial V_\theta}{\partial t}=-\frac{\nu}{a}V_\theta-\frac{f}{a}J_r\,,\qquad \langle V_\theta\rangle_t\approx-\sqrt{\pi}\frac{\Delta t}{t_p}\frac{f}{\nu}J_f A_{\max}\,。$$

$$\frac{\partial V_\theta'}{\partial t}=-\frac{\nu}{a}V_\theta'-\left(\frac{\nu}{a}\right)'V_\theta-\frac{f}{a}J_r'-\left(\frac{f}{a}\right)'J_r\,,\qquad \langle V_\theta'\rangle_t\approx-\frac{5\sqrt{\pi}}{2r_s}\frac{\Delta t}{t_p}\frac{f}{\nu}J_f A_{\max}\,。$$

- Numerical solution $R_0=2\text{m}$， $r_s/R_0=0.1$， $\nu=5/\text{s}$， $fJ_f=2.0\times10^9\,\text{m/s}^2$

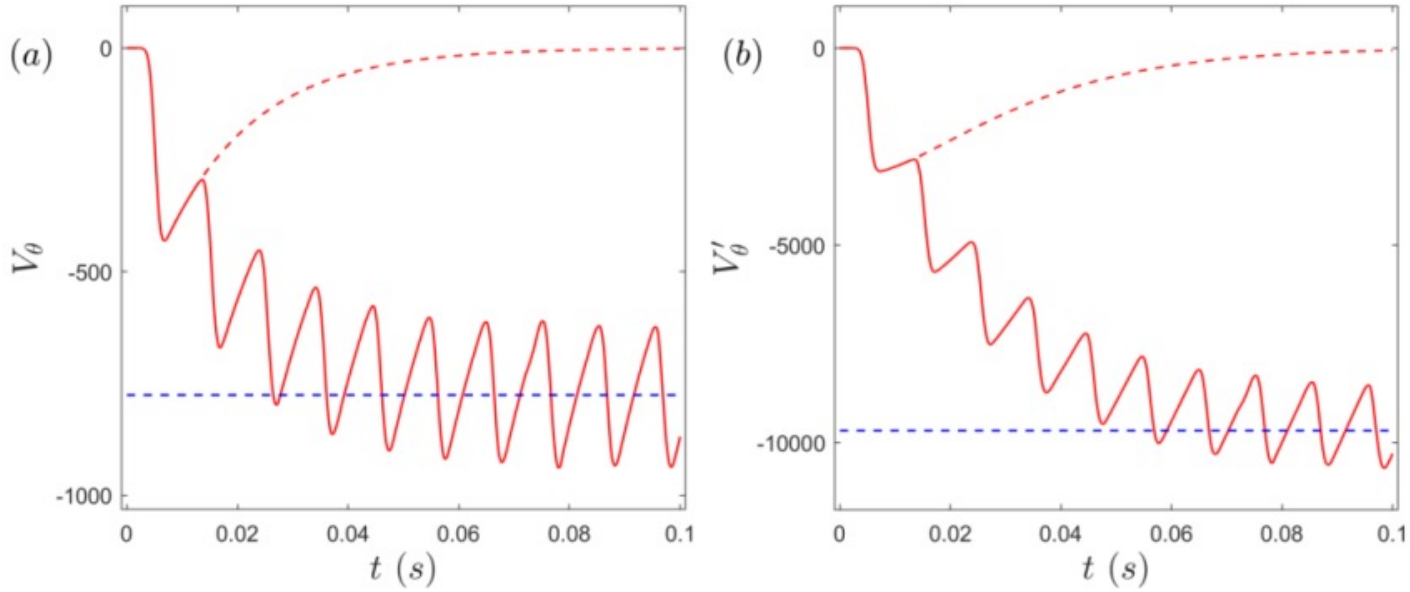

Theoretical model: Poloidal rotation driven by EP radial current

- Numerical solution

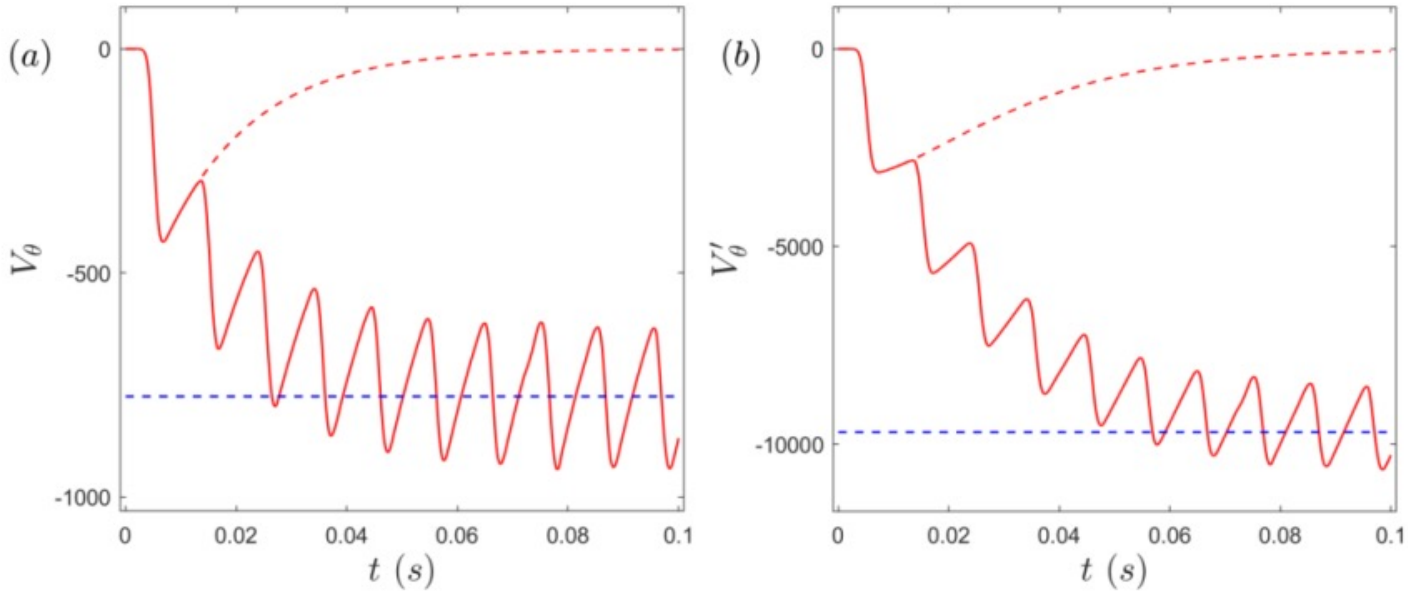

- Approximate solution $D \ll A_{\max} Z \beta_{\max}$

$$\left\langle \left| V'_\theta \right| \right\rangle_t \approx \frac{5\sqrt{\pi}}{4.4} \frac{\varepsilon^{3/2}}{q^2} \frac{\Omega_{\mathrm{ep}}}{\nu_{ii}} \frac{v_A^2}{v_{\mathrm{ep}}^2} \frac{D}{2}$$

The flow shear is independent of four of five parameters $D, Z, \beta_{\mathrm{crit}}, \beta_{\max}, \Gamma$

Flow shear is only dependent on D

$$\left\langle \left| V_\theta' \right| \right\rangle_t \approx \frac{5\sqrt{\pi}}{8.8} \frac{\epsilon^{3/2}}{q^2} \frac{\Omega_{\mathrm{ep}}}{\nu_{ii}} \frac{v_A^2}{v_{\mathrm{ep}}^2} \frac{\Delta t}{t_p} Z \beta_{\max} A_{\max}, \tag{2.19}$$

where $v_A \equiv B_0/\sqrt{\mu_0 n_i m_i}$ is the Alfvén velocity, $v_{\mathrm{ep}} \equiv \sqrt{T_{\mathrm{ep}}/m_{\mathrm{ep}}}$ is the EP thermal velocity, $\Omega_{\mathrm{ep}} \equiv q_{\mathrm{ep}} B_0/m_{\mathrm{ep}}$ is the EP gyrofrequency. This quantitative formula can be further simplified when D is small enough, $D \ll A_{\max} Z \beta_{\max}$. By using the relations given by (2.5)–(2.7*a*,*b*), the burst width can be approximated as $\Delta t \approx \sqrt{2/(\Gamma A_{\max} Z \beta_{\max})}$, because most of the time $A \ll A_{\max}$, the $A Z \beta_{\max}$ term in the integrand of (2.6) can be neglected; hence, the integral is solved analytically, $t_p \approx 2\sqrt{2 A_{\max} Z \beta_{\max}/\Gamma}/D$. As a result, we obtain $\Delta t/t_p \approx D/(2 A_{\max} Z \beta_{\max})$ and

$$\left\langle \left| V_\theta' \right| \right\rangle_t \approx \frac{5\sqrt{\pi}}{17.6} \frac{\epsilon^{3/2}}{q^2} \frac{\Omega_{\mathrm{ep}}}{\nu_{ii}} \frac{v_A^2}{v_{\mathrm{ep}}^2} D, \tag{2.20}$$

Theoretical model: Ion transport model

- Temporal evolution of ITG fluctuation level and ion pressure gradient [1]

$$\frac{\partial E}{\partial t} = \left(\gamma_0 N - \alpha_1 E - \alpha_2 V_E'^2\right) E \, ,$$

$$\frac{\partial N}{\partial t} = S - \left(D_n + D_a E\right) N \, ,$$

Where E is turbulence energy, N is the normalized pressure gradient

[1] P. H. Diamond, V. B. Lebedev, D. E. Newman, et. al., Dynamics of Transition to Enhanced Confinement in Reversed Magnetic Shear Discharges. Phys. Rev. Lett. 78, 1472 (1997).

Theoretical model: Ion transport model

- Temporal evolution of ITG fluctuation level and ion pressure gradient [1]

$$\frac{\partial E}{\partial t} = \left(\gamma_0 N - \alpha_1 E - \alpha_2 V_E'^2\right) E \text{ ,}$$

$$\frac{\partial N}{\partial t} = S - \left(D_n + D_a E\right) N \text{ ,}$$

[1] P. H. Diamond, V. B. Lebedev, D. E. Newman, et. al., Dynamics of Transition to Enhanced Confinement in Reversed Magnetic Shear Discharges. Phys. Rev. Lett. 78, 1472 (1997).

- Radial ion force balance equation $V_E = V_\theta - \frac{B_\theta}{B} V_\varphi - \frac{1}{eBn_i} \frac{dP_i}{dr}$。 $V_E' \approx V_\theta'$

- Low-confinement solution $(E,N) = (E_L, N_L)$， $V_\theta' \approx 0$， $E_L = \gamma_0 N_L / \alpha_1$， $S = \left(D_n + D_a E_L\right) N_L$；

- High-confinement solution $(E,N) = (E_H, N_H)$， $E_H \approx 0$， $N_H = S / D_n$。 $|V_\theta'| \geq V_{\theta,c}' \equiv \gamma_0 \sqrt{S / D_n}$。

Zero-dimensional model

$$\frac{d\beta_{\mathrm{ep}}}{dt} = D - AZ\beta_{\max} H\left(\beta_{\mathrm{ep}} - \beta_{\min}\right),$$

$$\frac{dA}{dt} = A\Gamma\left(\beta_{\mathrm{ep}} - \beta_{\mathrm{crit}}\right),$$

$$\frac{\partial V_\theta}{\partial t} = -\frac{\nu}{a}V_\theta - \frac{f}{a}J_r,$$

$$\frac{\partial V_\theta'}{\partial t} = -\frac{\nu}{a}V_\theta' - \left(\frac{\nu}{a}\right)' V_\theta - \frac{f}{a}J_r' - \left(\frac{f}{a}\right)' J_r,$$

$$\frac{\partial E}{\partial t} = \left(\gamma_0 N - \alpha_1 E - \alpha_2 V_\theta'^2\right)E$$

$$\frac{\partial N}{\partial t} = S - \left(D_n + D_a E\right)N$$

- Initial condition $A = A_{\min}$, $\beta_{\mathrm{ep}} = \beta_{\mathrm{crit}}$, $V_\theta' = 0$, $E = E_L = 0.06$, $N = N_L = 0.6$ 。
- Study the key parameter ($D, Z, \beta_{\mathrm{crit}}, \beta_{\max}, \Gamma$) to high-confinement solution: $N \rightarrow N_H = 2$

Numerical results

- Deposition rate of trapped EP within the q=1 surface: D
- As D increases, $|V'_\theta|$ grows linearly, the turbulent fluctuation E is suppressed, the ion pressure gradient N achieves a high-confinement solution

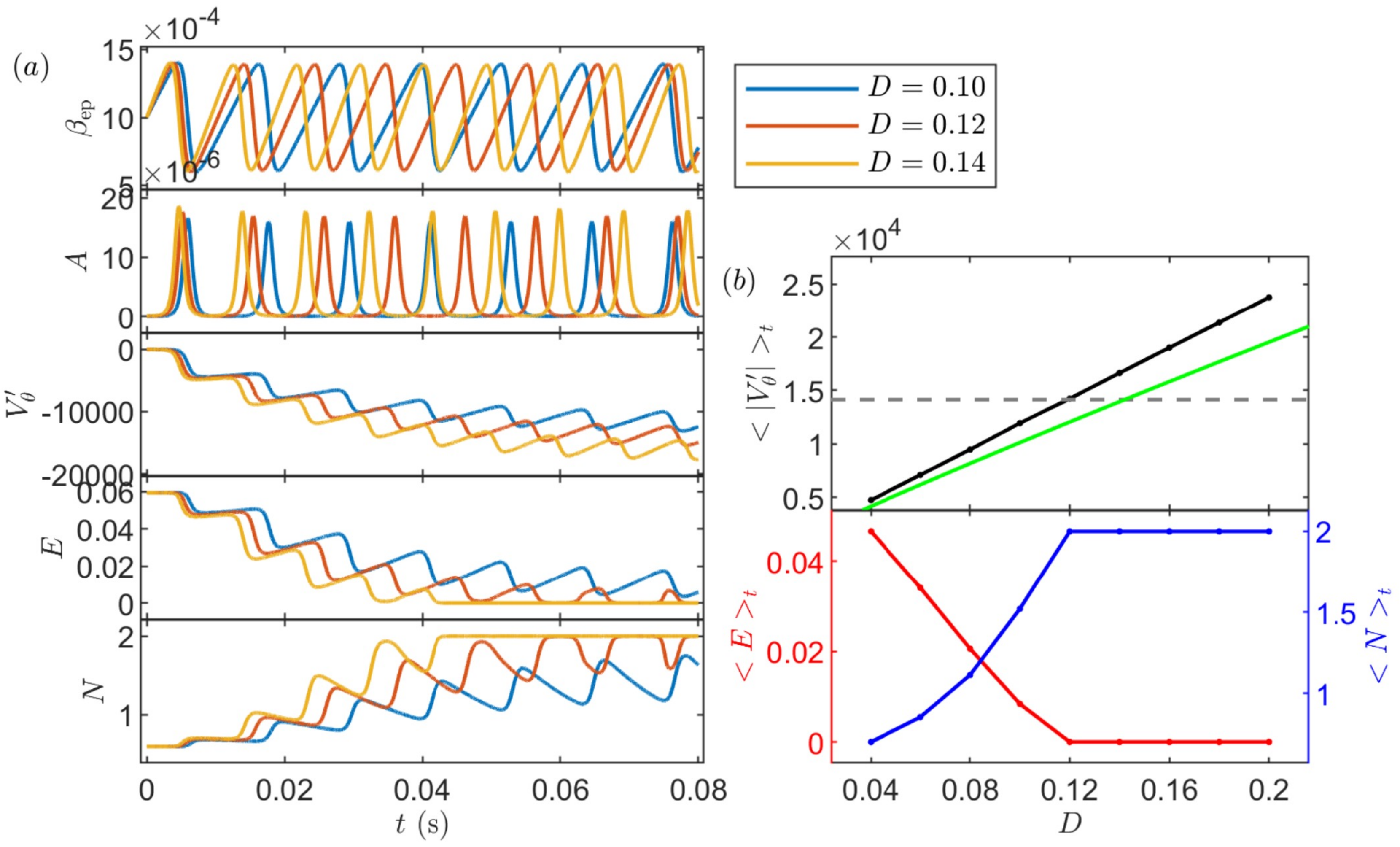

FIGURE 3. (a) Temporal evolutions of β_{ep}, A, V'_θ, E and N for $D = 0.10$, $D = 0.12$, and $D = 0.14$, (b) average values of $|V'_\theta|$, E and N over $t = 0.1 - 0.2$s with D increasing.

The steady flow shear is independent of the EP loss rate Z

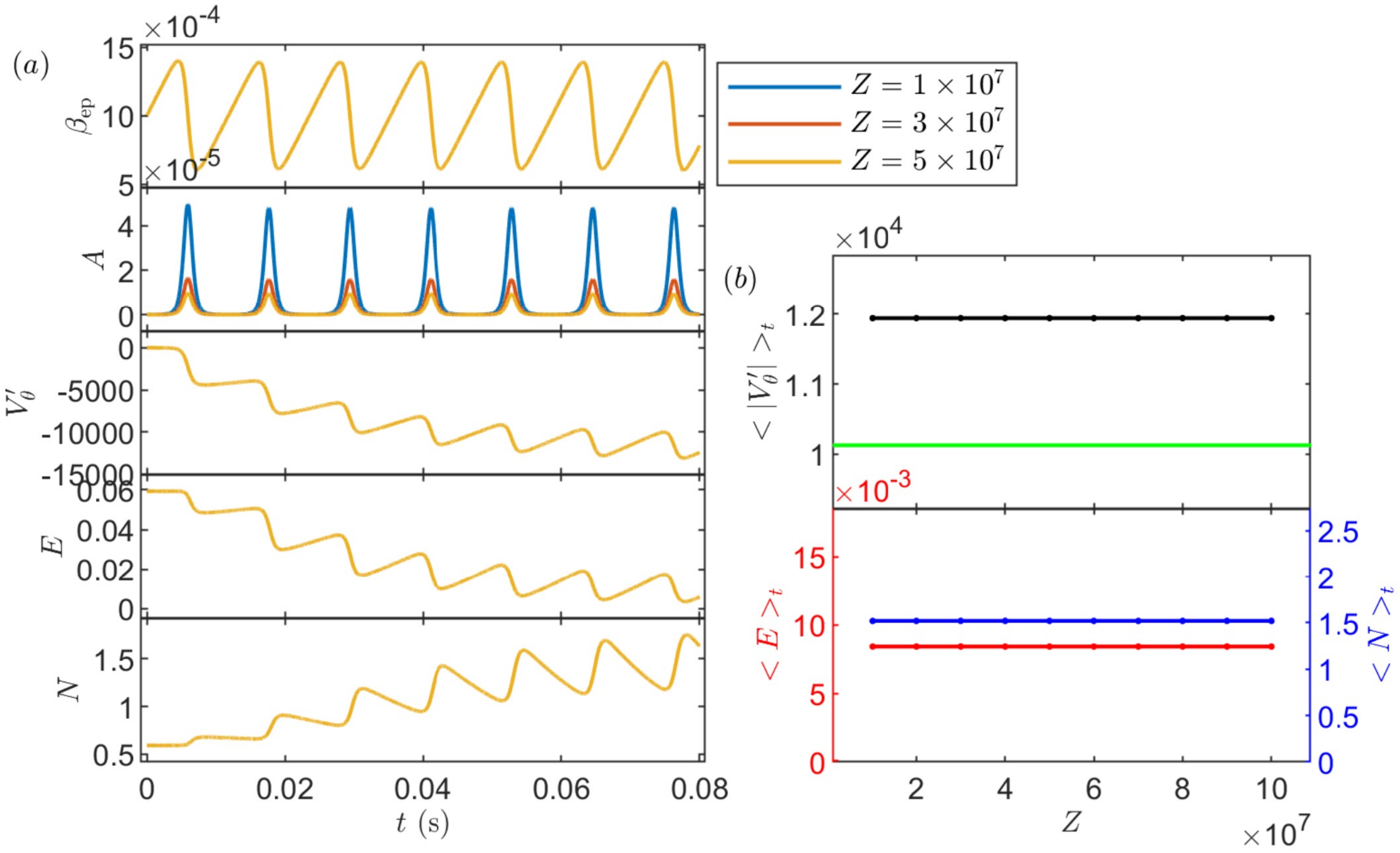

FIGURE 4. (a) Temporal evolutions of β_{ep}, A, V'_θ, E and N for $Z = 10^7$, $Z = 3 \times 10^7$, and $Z = 5 \times 10^7$, (b) average values of $|V'_\theta|$, E and N over $t = 0.1 - 0.2$s with Z increasing.

- The steady flow shear is nearly independent of the EP resonant drive coefficient Γ

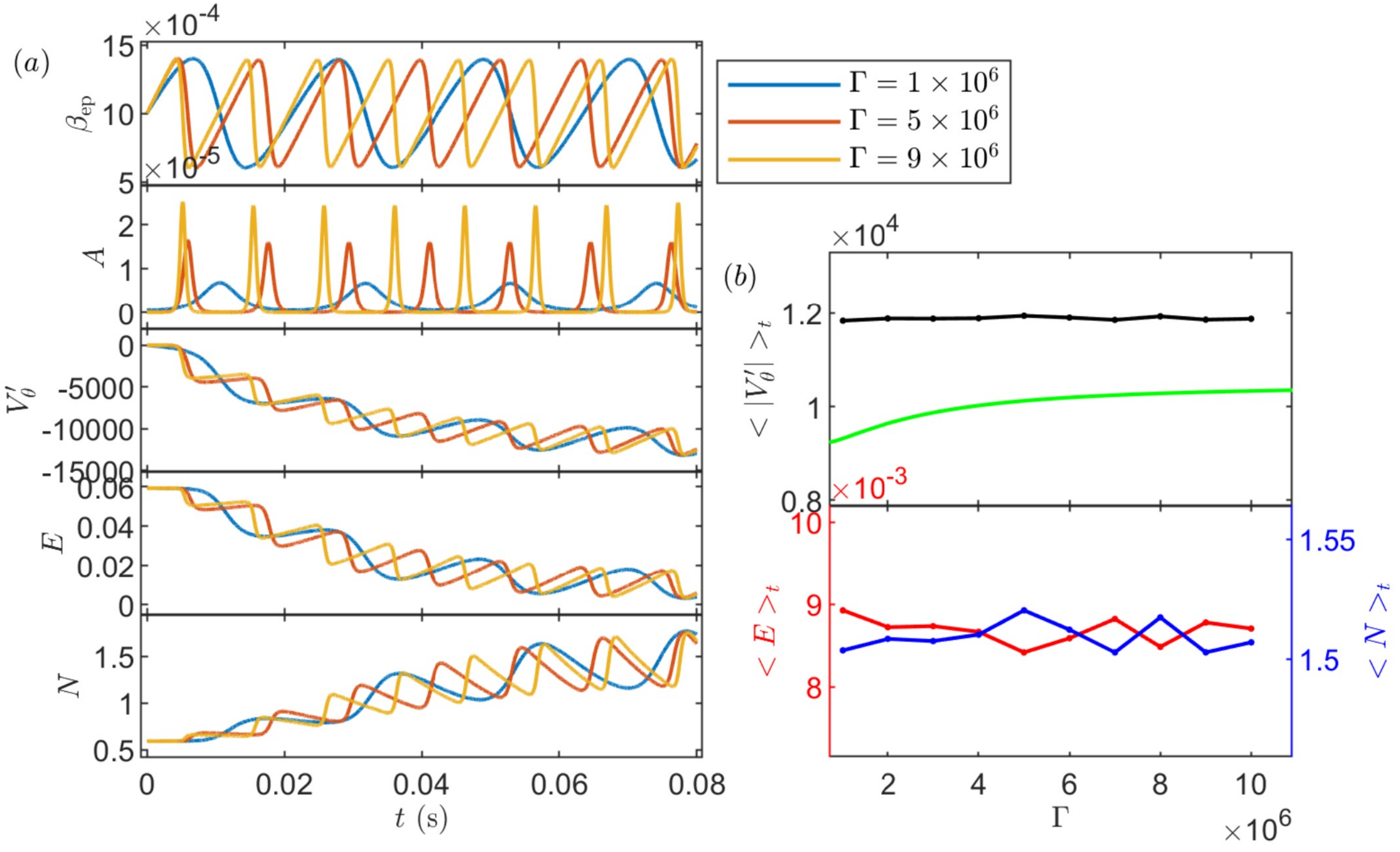

FIGURE 5. (a) Temporal evolutions of $\beta_{\rm ep}$, A, V'_θ, E and N for $\Gamma = 10^6$, $\Gamma = 5 \times 10^6$, and $\Gamma = 9 \times 10^6$, (b) average values of $|V'_\theta|$, E and N over $t = 0.1 - 0.2$s with Γ increasing.

- The steady flow shear is nearly independent of EP beta maximum: $\beta_{\max}$

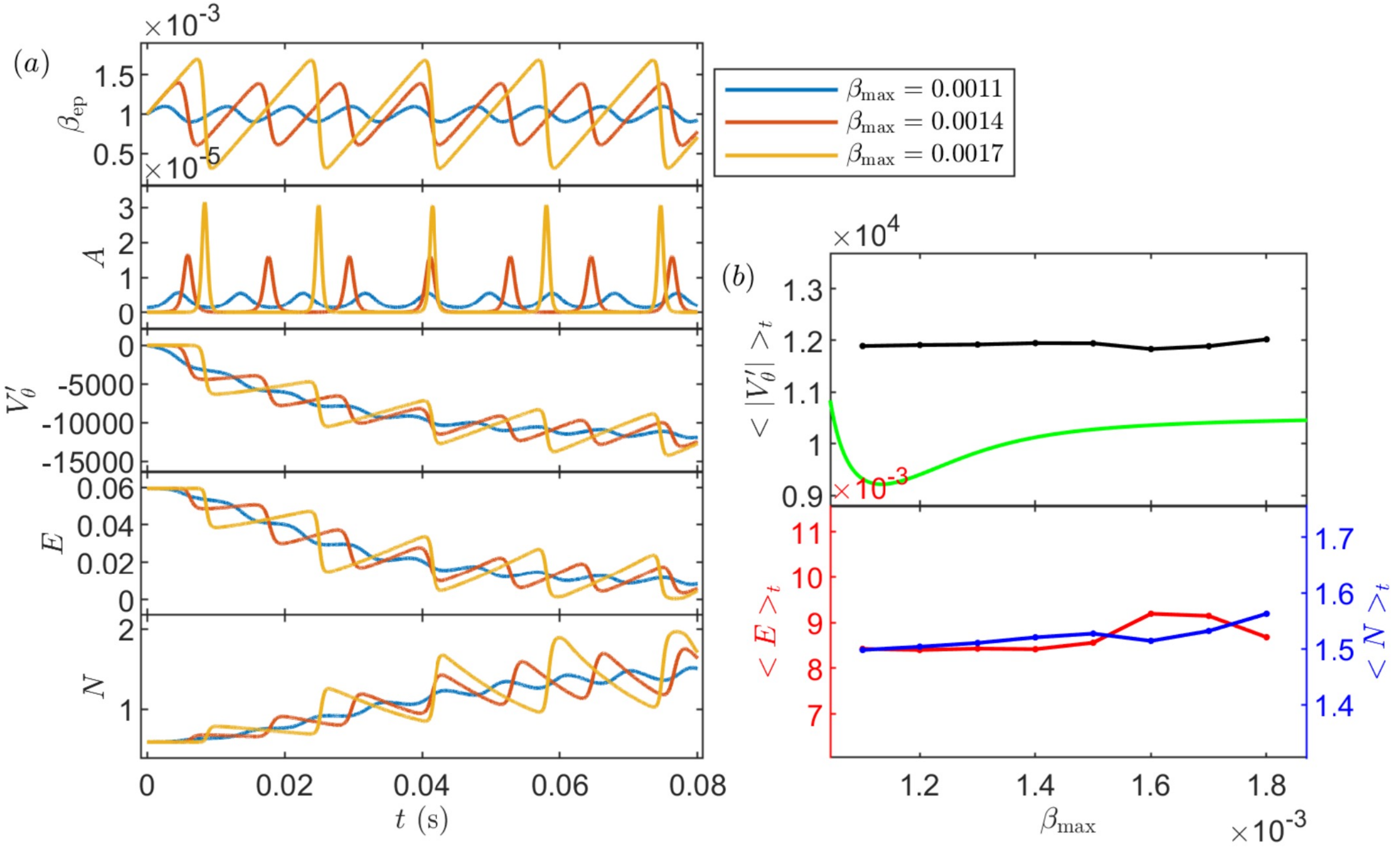

FIGURE 6. (a) Temporal evolutions of β_{ep}, A, V'_θ, E and N for $\beta_{\max} = 0.0011$, $\beta_{\max} = 0.0014$, and $\beta_{\max} = 0.0017$, (b) average values of $|V'_\theta|$, E and N over $t = 0.1 - 0.2$s with $\beta_{\max}$ increasing.

- The steady flow shear is nearly independent of excitation threshold of fishbone: β_{crit}

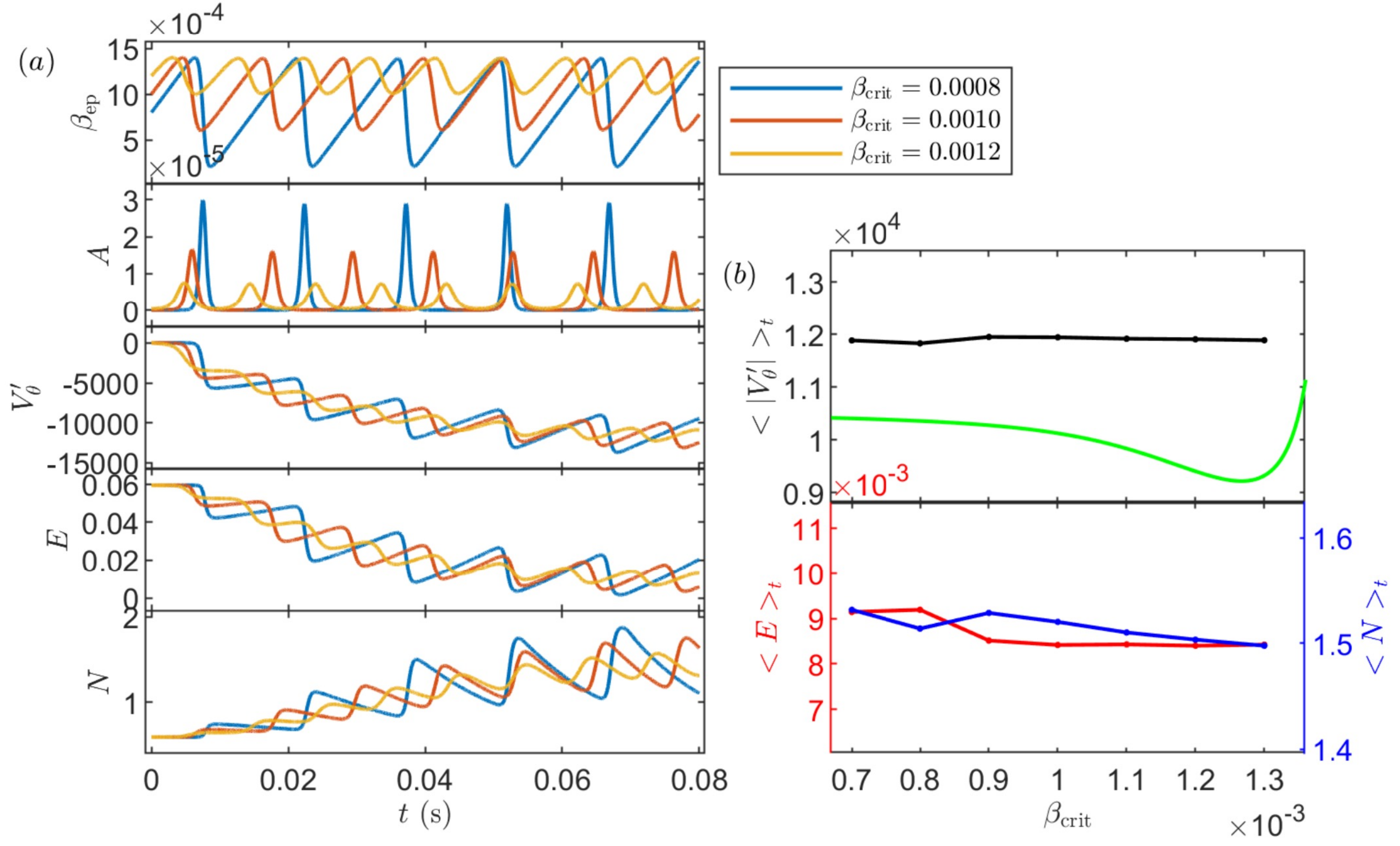

FIGURE 7. (a) Temporal evolutions of β_{ep}, A, V'_θ, E and N for $\beta_{crit} = 0.0008$, $\beta_{crit} = 0.001$, and $\beta_{crit} = 0.0012$, (b) average values of $|V'_\theta|$, E and N over $t = 0.1 - 0.2$s with β_{crit} increasing.

- The effects of EP slowing-down

$$\frac{d\beta_{\rm ep}}{dt} = D - AZ\beta_{\rm max}H(\beta_{\rm ep} - \beta_{\rm min}) - \frac{\beta_{\rm ep}}{\tau_s}$$

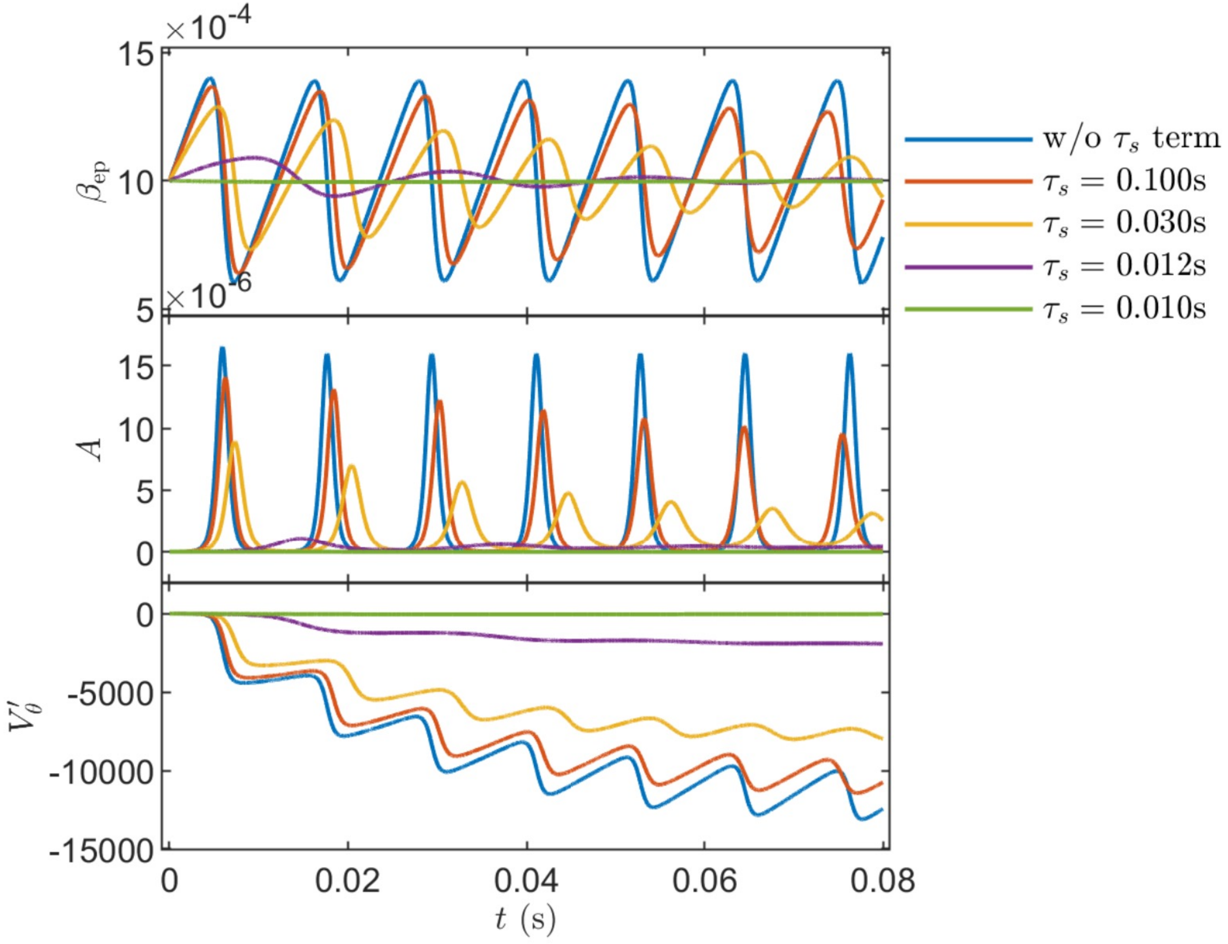

FIGURE 8. Numerical solution of predator-prey model and poloidal flow shear with different τ_s, other parameters are the same as in Figure 1 and Figure 2.

A figure of merit for fishbone stabilization of turbulence

$$\frac{|V_\theta'|}{\gamma_{\mathrm{ITG}}} \propto \frac{\epsilon^{3/2}}{q^2}\frac{\bar{n}_{\mathrm{ep}}}{n_i}\frac{L_{P_i}}{\rho_i},$$

$$Q_{\mathrm{fishbone}} = \frac{\epsilon^{3/2}}{q^2}\frac{\bar{n}_{\mathrm{ep}}}{n_i}\frac{L_{P_i}}{\rho_i}$$

Summary and Conclusions

- Fishbone dynamics, five key parameters: $D, Z, \beta_{\text{crit}}, \beta_{\max}, \Gamma$

- EP transport leads to radial current, proportional to the fishbone amplitude

- Quasi-neutrality condition, there must be a compensating bulk plasma return current, which can drive plasma poloidal rotation through $\mathbf{J}\times\mathbf{B}$ torque

- Steady poloidal flow can built up on condition that the burst frequency is greater than the poloidal flow damping rate

$$\left\langle \left| V_\theta' \right| \right\rangle_t \approx \frac{5\sqrt{\pi}}{4.4} \frac{\varepsilon^{3/2}}{q^2} \frac{\Omega_{\text{ep}}}{\nu_{ii}} \frac{v_A^2}{v_{\text{ep}}^2} \frac{D}{2}$$

- A figure of merit for fishbone stabilization of turbulence

$$Q_{\text{fishbone}} = \frac{\epsilon^{3/2}}{q^2} \frac{\bar{n}_{\text{ep}}}{n_i} \frac{L_{P_i}}{\rho_i}$$

Introduction: motivation for developing GMEC

- Energetic particle (EP) physics is crucial for burning plasmas:
  - EP-driven Alfvenic modes can strongly modify alpha particle distribution and induce alpha particle losses in burning plasmas ;
  - EP can have significant effects on thermal plasmas.

- The goal of this work is development of a highly efficient code for simulating energetic particle-driven Alfven modes and energetic particle transport in burning plasmas such as ITER;

- An initial version of GMEC has been developed based on gyrokinetic-MHD hybrid model. Work is in progress for adding fluid nonlinear physics as well as applying code to present tokamak experiments and future burning plasmas.

P. Y. Jiang et al, Phys. Plasmas 31, 073904 (2024
Z.Y. Liu et al, Phys. Plasmas 31, 073905 (2024)

Comparison with existing hybrid codes

codes	model	type	Numerical methods
MEGA	Kinetic-MHD	hybrid	explicit, finite difference, PIC
M3D-K	Kinetic-MHD	**hybrid**	Semi-implicit, finite element, PIC
M3D-C1-K	Kinetic-MHD	**hybrid**	Semi-implicit, finite element, PIC
NIMROD	Kinetic-MHD	**hybrid**	Semi-implicit, finite element, PIC
CLT-K	Kinetic-MHD	**hybrid**	Explicit, finite difference, PIC
GMEC	Gyrokinetic-MHD	hybrid	Explicit, finite difference, PIC Field-aligned coordinates

Compared with existing hybrid codes, GMEC has more physics, and is highly optimized for computational efficiency. GMEC uses field-aligned coordinates and symbolic method for coding.

Gyrokinetic MHD Hybrid Equations

$$\frac{d}{dt}\left[\frac{n_i e^2}{T_i}(1-\Gamma_0)\Phi\right]+\delta\boldsymbol{B}\cdot\nabla\frac{J_\parallel}{B}+(\boldsymbol{B}+\delta\boldsymbol{B})\cdot\nabla\frac{\delta J_\parallel}{B}+\frac{\boldsymbol{B}\times\nabla B}{B^3}\cdot\nabla\left(\delta P_\parallel+\delta P_\perp\right)=0,$$

$$\frac{d}{dt}=\frac{\partial}{\partial t}+\left(\frac{\boldsymbol{b}\times\nabla\Phi}{B}+\boldsymbol{V}_{*i}\right)\cdot\nabla,$$

$$\Gamma_0=e^{-k_\perp^2\rho_i^2}\mathrm{I}_0\left(k_\perp^2\rho_i^2\right),$$

$$\frac{\partial}{\partial t}A_\parallel=-\nabla_\parallel\Phi+\frac{1}{en_e}\nabla_\parallel P_e,$$

$$\frac{d}{dt}P_e=-\gamma\nabla\cdot\boldsymbol{V}_e P_e,$$

$$\boldsymbol{V}_e=\frac{\boldsymbol{E}\times\boldsymbol{B}}{B^2}-\frac{\delta J_\parallel}{en_e}\boldsymbol{b},$$

$$\frac{d\boldsymbol{X}}{dt}=\frac{1}{B^{**}}\left\{v_\parallel\boldsymbol{B}^*-\boldsymbol{b}\times\left[\langle\boldsymbol{E}\rangle-\frac{\mu}{q_s}\nabla\left(B+\langle\delta B\rangle\right)\right]\right\},$$

$$m_s\frac{dv_\parallel}{dt}=\frac{q_s}{B^{**}}\boldsymbol{B}^*\cdot\left[\langle\boldsymbol{E}\rangle-\frac{\mu}{q_s}\nabla\left(B+\langle\delta B\rangle\right)\right],$$

$$\boldsymbol{B}^*=\boldsymbol{B}+\langle\delta\boldsymbol{B}\rangle+\frac{mv_\parallel}{e}\nabla\times\boldsymbol{b},\quad B^{**}=\boldsymbol{B}^*\cdot\boldsymbol{b}。$$

$$\boldsymbol{E}=-\nabla\Phi-\frac{\partial A_\parallel}{\partial t}\boldsymbol{b},$$

$$\delta\boldsymbol{B}=\nabla\times\left(A_\parallel\boldsymbol{b}\right)。$$

Development of GMEC

- Field-aligned coordinates
- Discretization methods
- Compile-time Symbolic Solver (CSS)
- δf PIC method for solving the EP and thermal ion distributions
- Equilibrium interface with VMEC and DESC
- Code optimization

Symbolic implementation of GMEC

$$\nabla_\parallel = \vec{b}\cdot\nabla$$

```
auto Nabla_p = b*Nabla
```

$$\delta\bar{\omega} = \nabla\cdot\frac{1}{v_A^2}\nabla_\perp\delta\Phi$$

```
auto dw = Div*(_va2*Nabla*dPhi)
```

$$\delta J_\parallel = -\frac{1}{B}\nabla\cdot\left(B^2\nabla_\perp\left(\frac{\delta A_\parallel}{B}\right)\right)$$

```
auto dJp = - Div*(Bs2*Nabla*(dA/Bs))/Bs
```

$$\delta\vec{B} = \nabla\times\left(\delta A_\parallel\vec{b}\right)$$

```
auto dB = Cross(Nabla,dA*b)
```

$$\vec{v}_{*i} = \frac{1}{enB}\vec{b}\times\nabla \mathrm{P_i}$$

```
auto v_star = Cross(b,Nabla*Pi)
              /(e*n*Bs)
```

$$\vec{v}_{E\times B} = \frac{1}{B}\vec{b}\times\nabla\delta\Phi$$

```
auto v_EB = Cross(b,Nabla*Phi)/Bs
```

$$\vec{v}_d = \frac{1}{B}\vec{b}\times\vec{\kappa}$$

```
auto v_d = Cross(b,kappa)/Bs
```

$$\frac{\partial}{\partial t}\delta\bar{\omega} = -\vec{v}_{*i}\cdot\nabla\delta\bar{\omega} \quad + \delta\vec{B}\cdot\nabla\left(\frac{\mathrm{J}_\parallel}{B}\right) \quad + \vec{B}\cdot\nabla\left(\frac{\delta J_\parallel}{B}\right) \quad + 2\vec{v}_d\cdot\nabla_\perp\delta P$$

```
constexpr auto dw_dt = -v_star*Nabla*dw + dB*Nabla*(Jp/Bs) + Bs*b*Nabla*(dJ/Bs) + Ratio<2>{}*v_d*Nabla*dP
```

$$\frac{\partial}{\partial t}\delta A_\parallel = -\nabla_\parallel\delta\Phi \quad - \eta\delta J_\parallel \quad + \frac{P_e}{en_e^2B}\delta\vec{B}\cdot\nabla n_e \quad + \frac{P_e}{en_e^2}\vec{b}\cdot\nabla\delta n_e$$

```
constexpr auto dA_dt = -Nabla_p*dPhi - eta*dJp + Pe/(e*ne2*Bs)*dB*Nabla*ne + Pe/(e*ne2)*b*Nabla*dne
```

$$\frac{\partial}{\partial t}\delta P = -\vec{v}_{E\times B}\cdot\nabla(P_i + P_e) - 2\Gamma(P_i + P_e)\vec{v}_d\cdot\nabla\delta\Phi$$

```
constexpr auto dP_dt = -v_EB*Nabla*(Pi+Pe) -
        Ratio<2>{}*gamma*(Pi+Pe)*v_d*Nabla*dPhi
```

$$\frac{\partial}{\partial t}\delta n_e = -\vec{v}_{E\times B}\cdot\nabla n_e$$

```
constexpr auto dne_dt = -v_EB*Nabla*ne
```

A GPU version of GMEC has been developed with high efficiency

Shiyang Liu

理论算力	Float	Double
Intel Xeon Gold 6348	4.6 TFLOPS	2.3 TFLOPS
RTX4090	82.58 TFLOPS	1.29 TFLOPS
A800	19.49 TFLOPS	9.746 TFLOPS

$n = 6, TAE, 256\times64\times16$

$N_p = 1.6\times10^7$

$dt = 0.1R_0/v_A$, $t = 250R_0/v_A$

A800: $52.3s$

RTX4090: $59.5s$

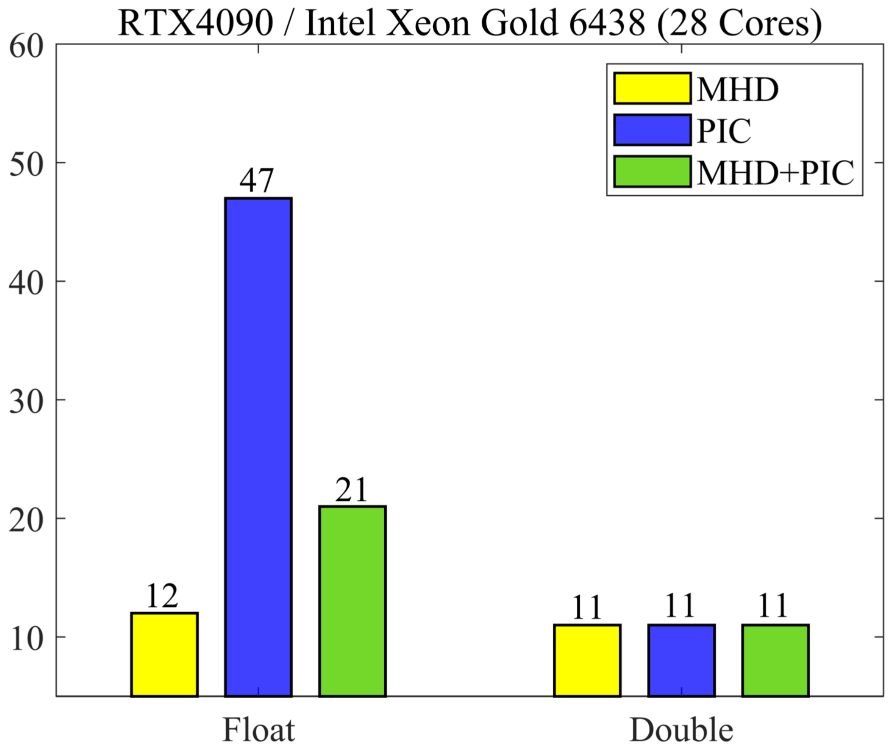

1个4090 ≈ 600核

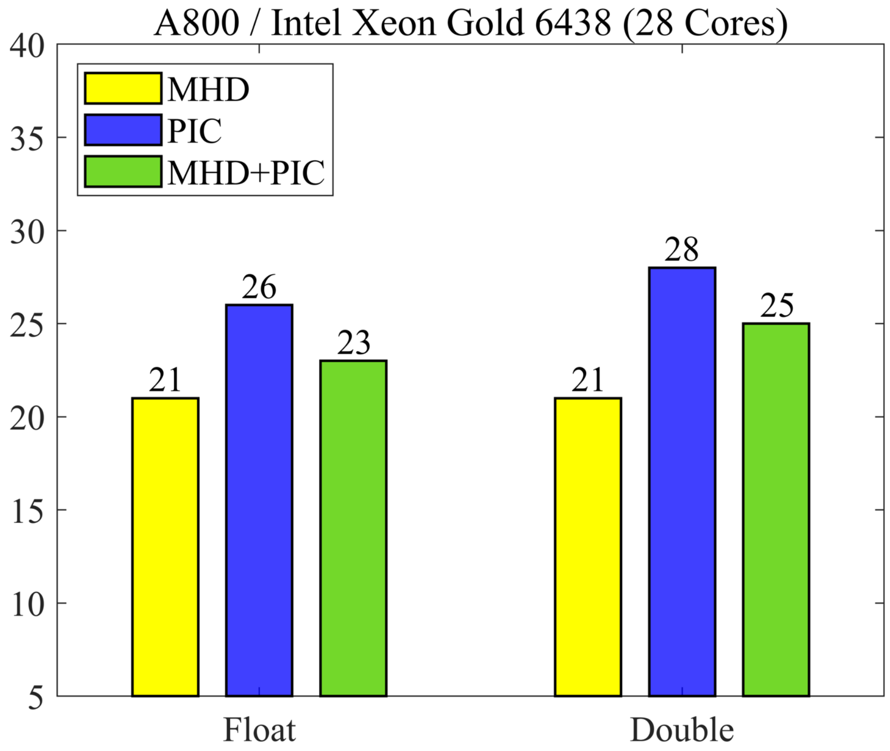

one A800 ≈ 640 cores

Verification of GMEC：RSAEs in DIII-D

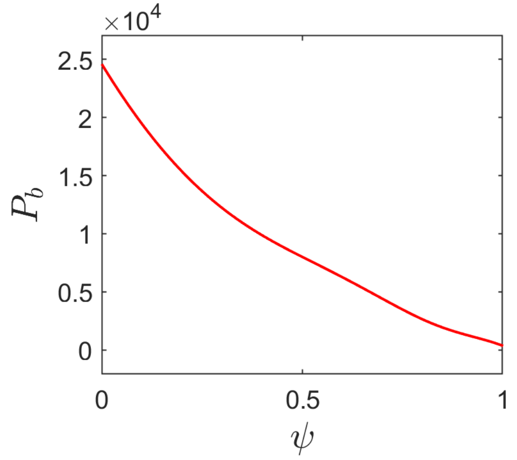

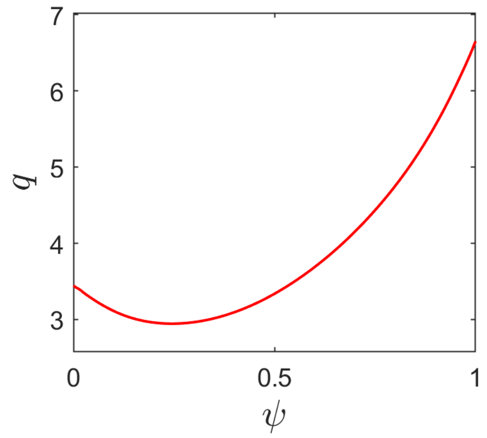

$q_{min} = 3$

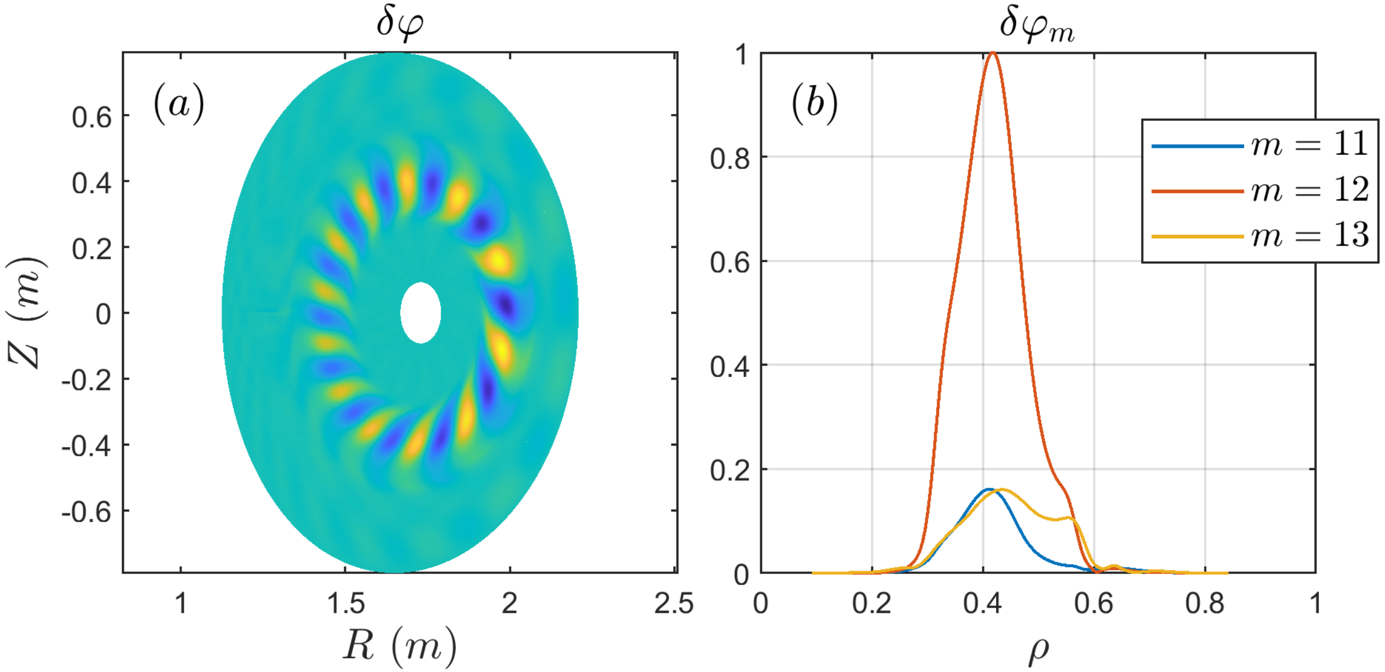

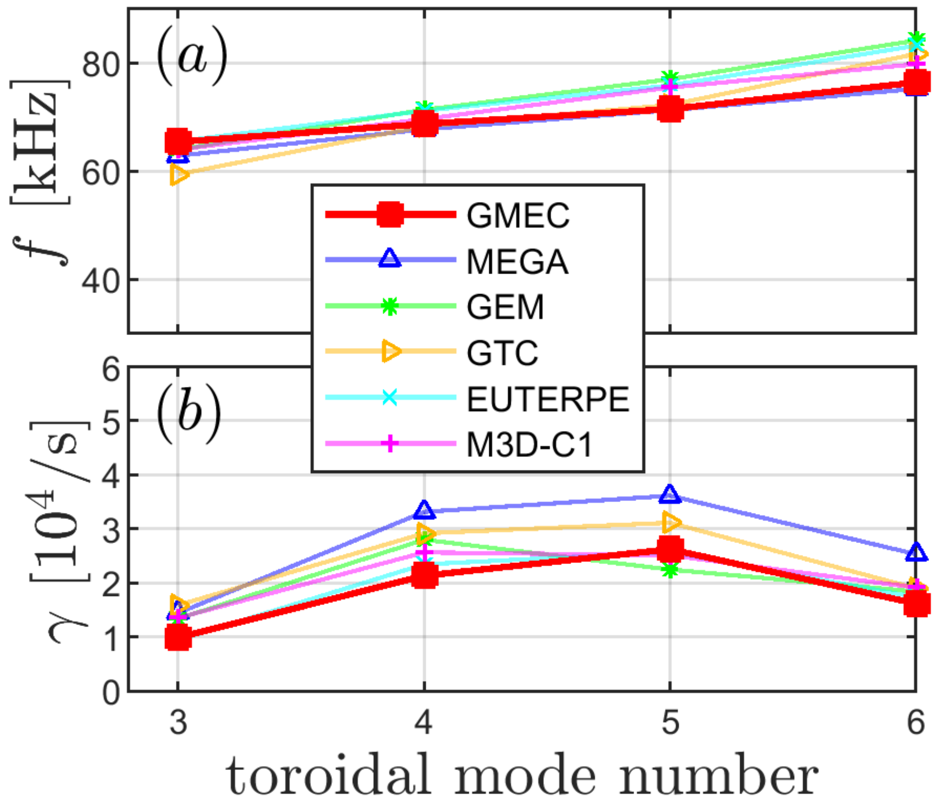

S. Taimourzadeh *et al* 2019 *Nucl. Fusion* **59** 066006

Verification of GMEC：n=6 TAE

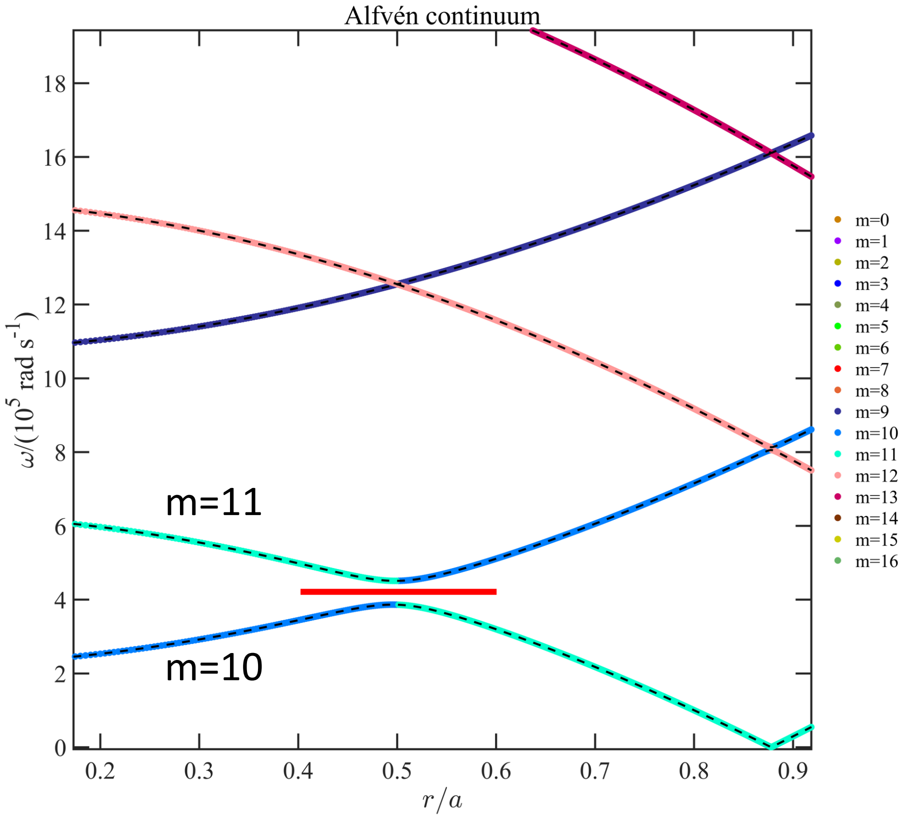

Continuum (MAS)
Gap range: [3.86,4.52]

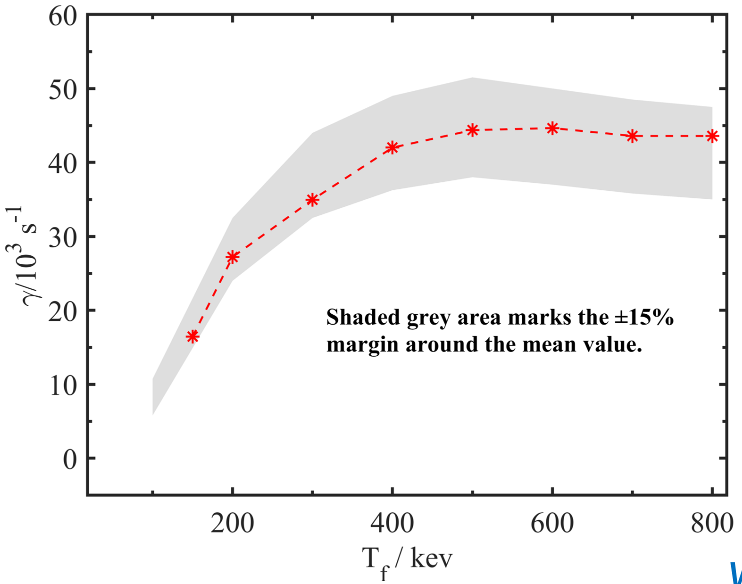

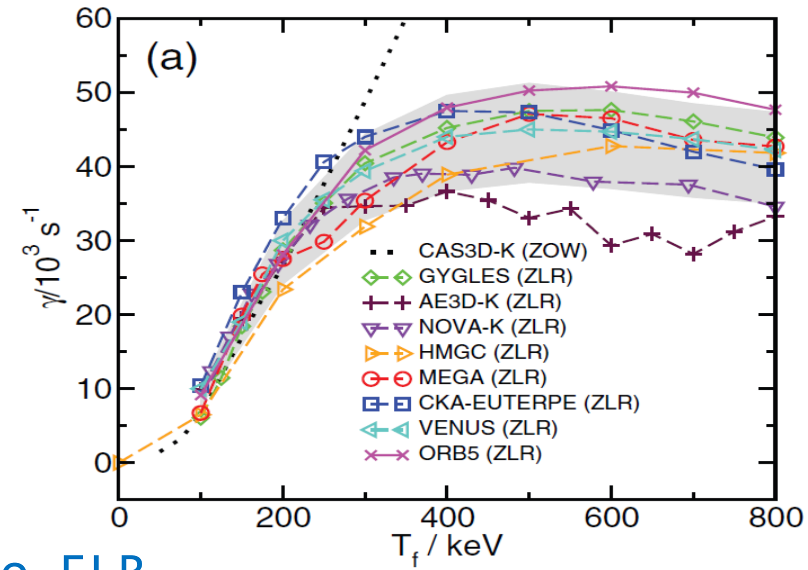

wo FLR

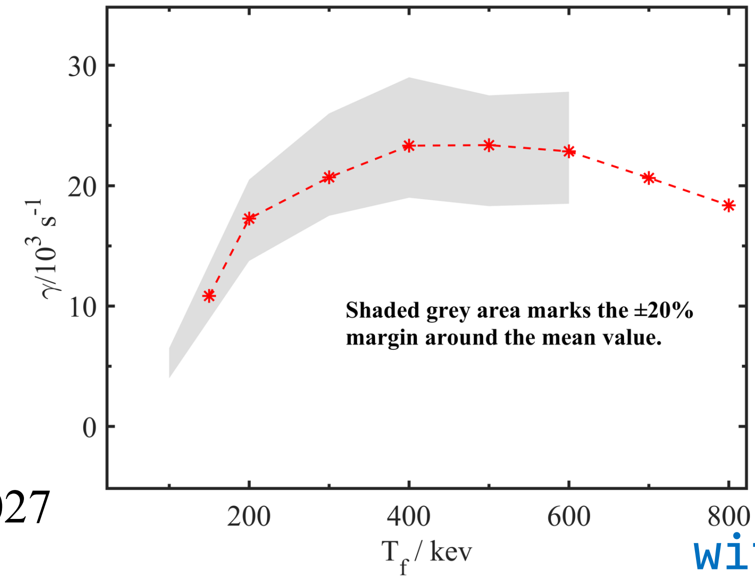

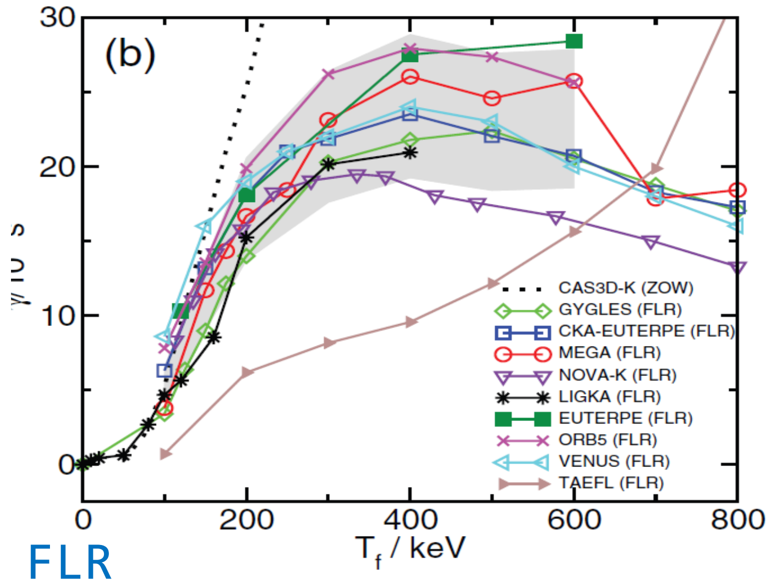

with FLR

A. Könies *et al* 2018 *Nucl. Fusion* **58** 126027

multi-n simulations

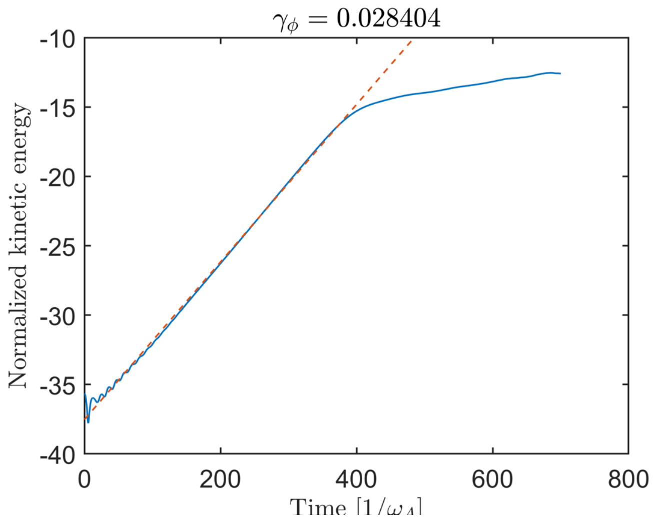

$t = 700R_0/v_A$

Linear phase

$n = 6$

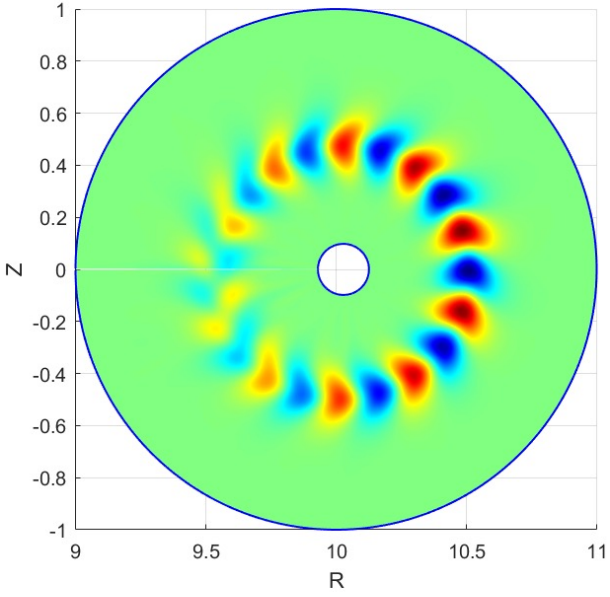

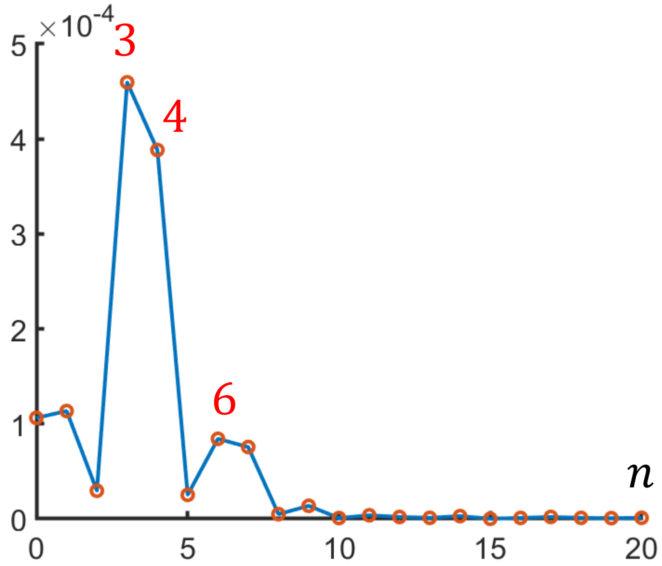

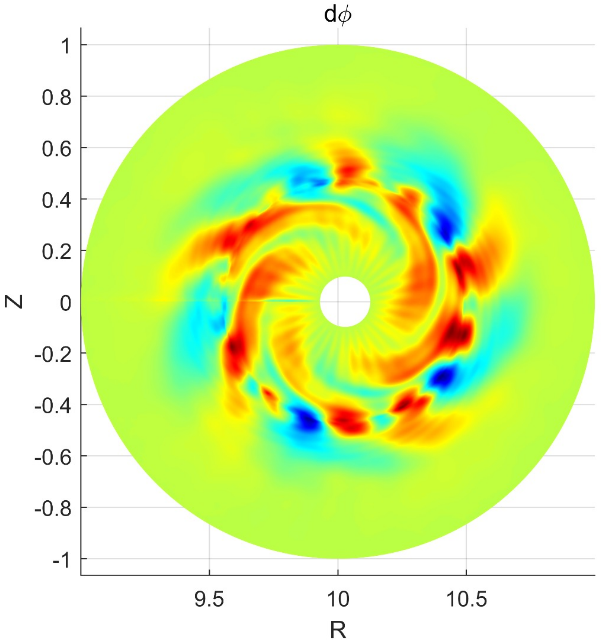

n total

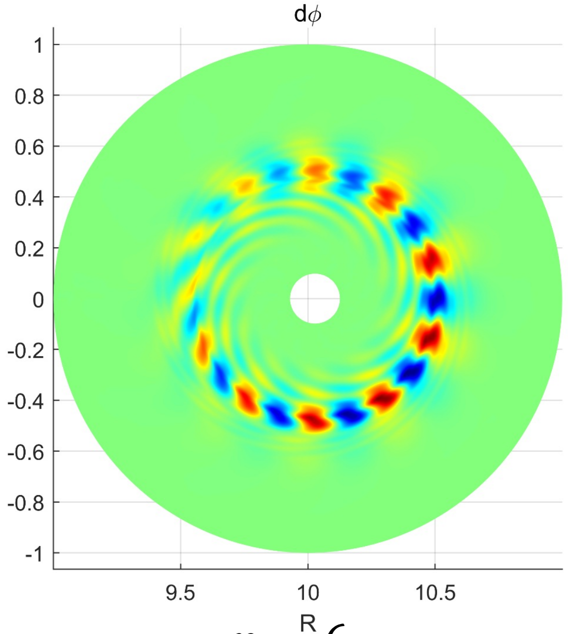

$n = 6$

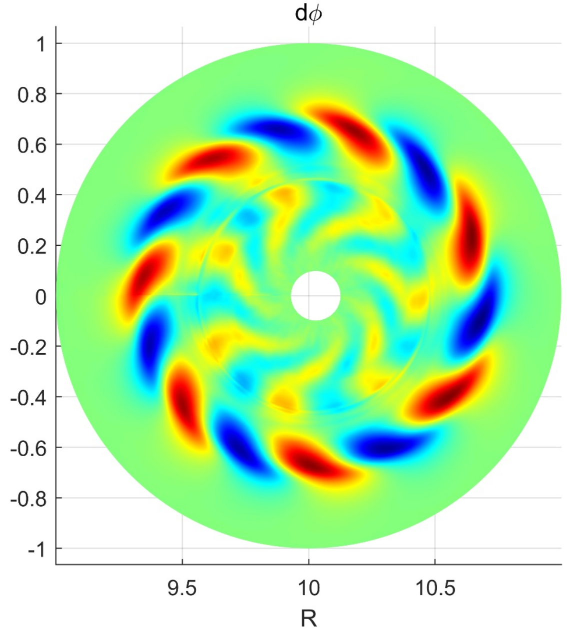

$n = 3$

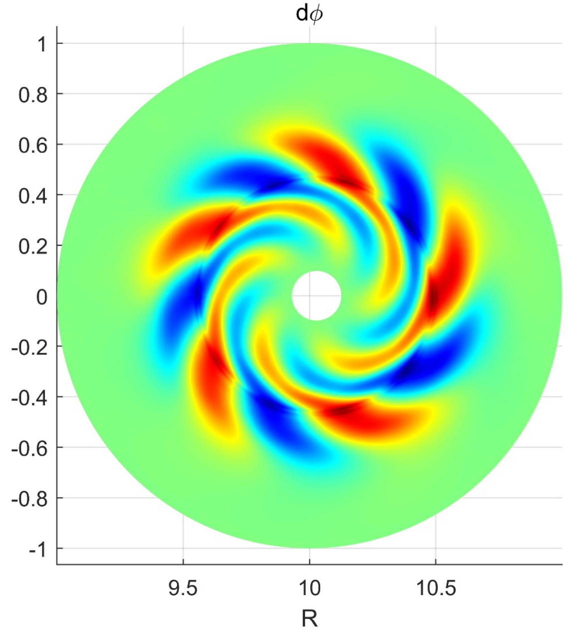

$n = 4$

n=30 mode in ITER (BAE)

N=30 Gamma=5/3 Frequency=65KHz

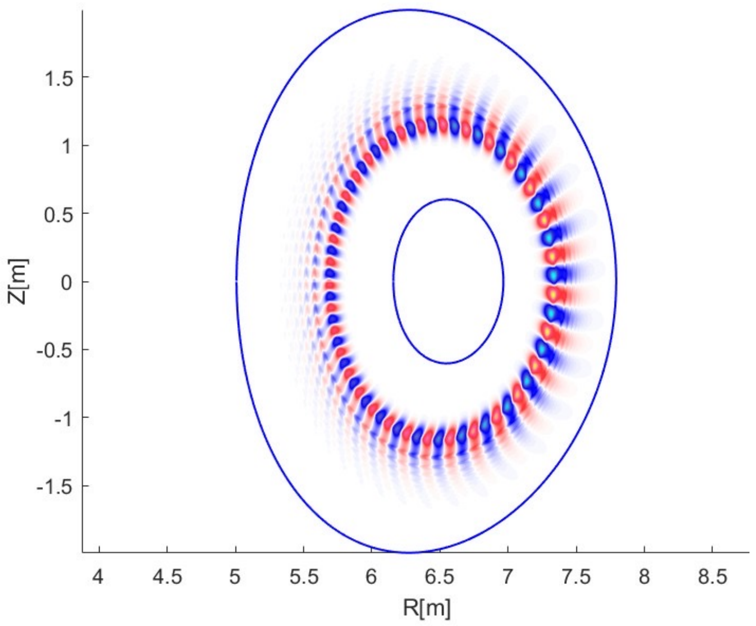

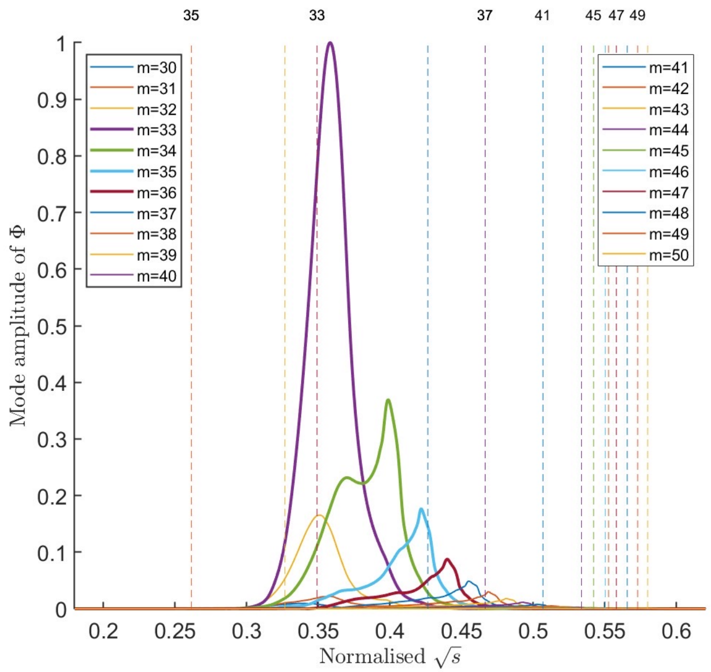

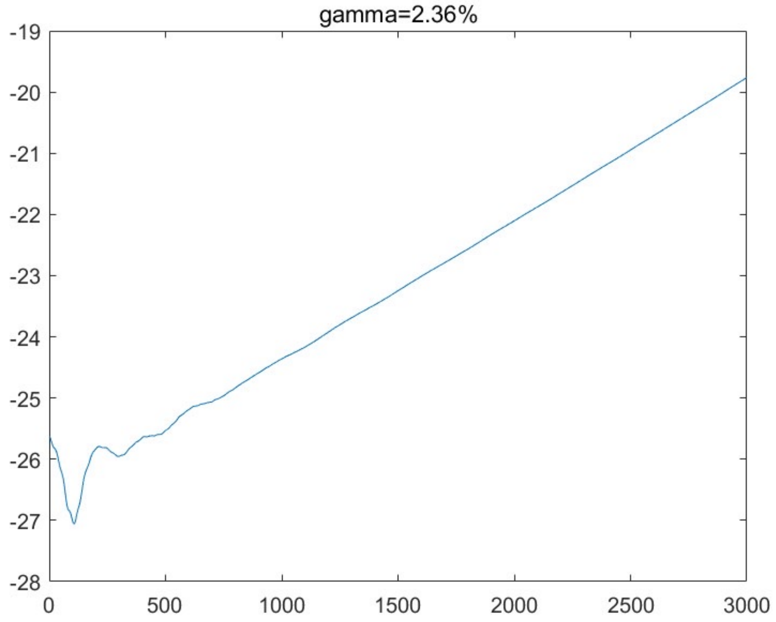

Summary II

- An initial version of GMEC has been developed for simulating EP-driven Alfven modes and EP transport in tokamak plasmas. Initial verifications have been done successfully.
- A Compile-time Symbolic Solver (CSS) has been developed to aid the development of GMEC. CSS simplifies the coding greatly with great efficiency and small probability for code errors. It also makes the code easily extensible.
- Initial results indicate GMEC is highly efficient and is significantly faster than existing codes.